Chapter 5
Shallow-Water Rogue Waves

When the sea becomes shallow, the water flow induced by surface waves is almost uniform with depth. Thus, properties of shallow water waves are radically different from those in deep water: the wave dispersion is weak, and waves now "feel" the seafloor. Nonlinearity leads to strong correlation between spectral components supporting existence of various wave shapes such as solitons, cnoidal waves, and undular bores. The interaction of water waves with variable bathymetry and coastal lines modifies the wave regime in shallow water and influences rogue wave formation. This chapter is devoted to the description of theoretical models of shallow-water freak waves.

5.1 Nonlinear Models of Shallow-Water Waves

The basic 3D hydrodynamic models are effective for studying wave processes in relatively small basins due to limited computer resources. This is why various depth-averaged models (2D) are popular to describe wind wave processes in the coastal zone of seas and oceans, and sometimes for transoceanic propagation of large-scale waves (such as a tsunami). A straightforward way to derive nonlinear dispersive models of shallow-water waves is to use the Euler equation written for potential flow

$$\mathbf{U} = \nabla\phi, \quad W = \partial\phi/\partial Z. \tag{5.1}$$

All vector operations hereafter act in the horizontal plane, so that $\nabla = (\partial/\partial X, \partial/\partial Y)^t, \Delta = \nabla\cdot\nabla$ and $\mathbf{U} = (U,V)$ (see geometry in Fig 2.1). Then, the Laplace equation (2.13) has the form

$$\Delta\phi + \frac{\partial^2\phi}{\partial Z^2} = 0, \tag{5.2}$$

with the boundary condition (2.31) at the uneven bottom, $Z = -D(X,Y)$,

$$\partial\phi/\partial Z + \nabla\phi\cdot\nabla D = 0, \tag{5.3}$$

and kinematic and dynamic conditions on the free surface, $Z = \eta(X,Y,T)$ (see Chap. 2),

C. Kharif et al., *Rogue Waves in the Ocean*, Advances in Geophysical and Environmental Mechanics and Mathematics, DOI 10.1007/978-3-540-88419-4_6,

$$\frac{\partial \phi}{\partial Z} = \frac{d\eta}{dT} = \frac{\partial \eta}{\partial T} + \nabla\phi \cdot \nabla\eta \text{ on } Z = \eta, \tag{5.4}$$

$$\frac{\partial \phi}{\partial T} + \frac{1}{2}\left(\frac{\partial \phi}{\partial Z}\right)^2 + g\eta = 0 \text{ on } Z = \eta. \tag{5.5}$$

Since potential flow is governed by a harmonic function, it can be differentiated with respect to all its arguments and expanded as a Taylor series with respect to the vertical coordinate centered at $Z = -D$,

$$\phi(X,Y,Z,T) = \sum_{n=0}^{\infty} q_n(X,Y,T)(Z+D)^n. \tag{5.6}$$

Substitution of Eq. (5.6) into the Laplace equation (5.2) yields the recurrence correlations for the unknown functions q_n,

$$(n+2)(n+1)q_{n+2} + \Delta q_n + 2(n+1)\nabla q_{n+1}\nabla D + (n+1)q_{n+1}\Delta D + (n+2)(n+1)q_{n+2}(\nabla D)^2 = 0, \tag{5.7}$$

so that only two of them (namely, q_0 and q_1) are independent. Specifically, q_2 is given by

$$q_2 = -\frac{\Delta q_0 + 2\nabla q_1 \nabla D + q_1 \Delta D}{2[1+(\nabla D)^2]}. \tag{5.8}$$

By substituting series (5.6) into the boundary condition on the bottom (5.3) and using Eq. (5.7), we may deduce the following relation between q_1 and q_0

$$q_1 = -\frac{\nabla q_0 \nabla D}{[1+(\nabla D)^2]}. \tag{5.9}$$

Thus, the series (5.6) is completely determined by only one function, $q_0(X,Y,T)$. Boundary conditions on the free surface (5.4) and (5.5) provide equations for η and ∇q_0. The physical meaning of ∇q_0 is the bottom velocity (for a flat floor). When the depth-averaged velocity

$$\mathbf{u}(X,Y,T) = \frac{1}{D+\eta}\int_{-D}^{\eta} \nabla\phi(X,Y,Z,T)dZ \tag{5.10}$$

is chosen as the "physical" horizontal velocity, then the value of ∇q_0 can be calculated from (5.6) approximately as

$$\nabla q_0 = \mathbf{u} + \frac{D+\eta}{2}\mathbf{u}\Delta D + (D+\eta)(\nabla D\nabla)\mathbf{u} + (\nabla D)^2\mathbf{u} + \frac{(D+\eta)^2}{6}\Delta\mathbf{u} + \ldots, \tag{5.11}$$

where the iteration procedure employs a small parameter D/λ, where λ is the wavelength characterizing the "shallowness" of long-water waves. After substitution of series (5.11), Eqs. (5.4) and (5.5) result in equations for the fully nonlinear

weakly dispersive theory (see details in Green and Naghdi 1976, and Zheleznyak and Pelinovsky 1985)

$$\frac{\partial \eta}{\partial T} + \nabla \cdot [(D+\eta)\mathbf{u}] = 0, \tag{5.12}$$

$$\frac{\partial \mathbf{u}}{\partial T} + (\mathbf{u}\nabla)\mathbf{u} + g\nabla\eta = \mathbf{F}, \tag{5.13}$$

where $\mathbf{F}$ characterizes weak dispersion

$$\mathbf{F} = \frac{1}{D+\eta}\nabla\left[\frac{(D+\eta)^3}{3}R + \frac{(D+\eta)^2}{2}Q\right] - \nabla D\left[\frac{D+\eta}{2}R + Q\right], \tag{5.14}$$

$$R = \frac{\partial}{\partial T}\nabla\cdot\mathbf{u} + (\mathbf{u}\nabla)\nabla\cdot\mathbf{u} - (\nabla\cdot\mathbf{u})^2, \quad Q = \frac{\partial \mathbf{u}}{\partial T}\nabla D + (\mathbf{u}\nabla)(\mathbf{u}\nabla D). \tag{5.15}$$

In fact, we may choose the particle velocity at any depth as a physical variable, and recalculate ∇q_0 from (5.6); this leads to other forms of nonlinear dispersive equations for long waves (Wei et al. 1995, Madsen and Schaffer 1998, Agnon et al. 1999, Chen et al. 2000, Kim et al. 2003, Madsen et al. 2002, 2003). For most of them, the obtained linear dispersion relation has a Padé-polynomial form like (Madsen et al. 2003)

$$\frac{\Omega^2}{gDK^2} = \frac{1 + K^2D^2/6 + K^4D^4/120}{1 + K^2D^2/2 + K^4D^4/24}, \tag{5.16}$$

which is a very good approximation of the exact dispersion relation (2.52) in a relatively wide range of water depths KD (until depth of order $KD \approx 10$). Therefore, models of this type might be called fully nonlinear and dispersive systems of long waves (Boussinesq-like systems).

For the case of weakly nonlinear and weakly dispersive waves, all the Boussinesq-like models reduce to the Peregrine system (Peregrine 1967, 1972)

$$\begin{aligned} &\frac{\partial \eta}{\partial T} + \nabla\cdot[(D+\eta)\mathbf{u}] = 0, \\ &\frac{\partial \mathbf{u}}{\partial T} + (\mathbf{u}\nabla)\mathbf{u} + g\nabla\eta = \frac{D}{2}\frac{\partial}{\partial T}\left[\nabla(\nabla\cdot(\mathbf{u}D)) - \frac{D}{3}\nabla(\nabla\cdot\mathbf{u})\right]. \end{aligned} \tag{5.17}$$

If the wave propagates mostly in one direction, and the bottom slope is small enough to neglect the wave reflection, the Peregrine system can be reduced to the famous Korteweg-de Vries and Kadomtsev-Petviashvili equations. At first, system (5.17) can be re-written in the form of a nonlinear wave equation for the water surface elevation, η,

$$\frac{\partial^2 \eta}{\partial T^2} - \nabla\cdot\left[C^2\nabla\eta\right] = \Pi\{\eta,\mathbf{u}\} := -\nabla\cdot\left[\frac{\partial(\eta\mathbf{u})}{\partial T} + D\mathbf{F} - D(\mathbf{u}\nabla)\mathbf{u}\right], \tag{5.18}$$

where C is the long-wave speed, $C^2 = gD$. The function $\prod$ specifies nonlinear and dispersive terms that are weak. Let us introduce a new temporal variable

$$s = \tau(X,Y) - T, \tag{5.19}$$

where the function τ will be determined later. With these new variables, Eq. (5.18) reads

$$\left[1 - C^2(\nabla\tau)^2\right]\frac{\partial^2\eta}{\partial s^2} - \frac{\partial}{\partial s}\left[2C^2\nabla\tau\nabla\eta + \eta\nabla\cdot\left(C^2\nabla\tau\right)\right] - \nabla\cdot\left(C^2\nabla\eta\right) = \Pi. \tag{5.20}$$

When curvatures of the wave front and bottom slope are small (this assumption is normal for the ray theory), the elevation is a fast function of s and a slow function of spatial coordinates. Due to this, the last term on the LHS of Eq. (5.20) may be neglected. Owing to the weakness of nonlinearity and dispersion on the RHS of (5.20), a linear relation of long waves

$$\mathbf{u} = g\nabla\tau\eta \tag{5.21}$$

can be applied as follows from Eq. (5.17). As a result, Eq. (5.20) splits into a system of two equations for τ and η (see Engelbrecht et al. 1988 and Dingemans 1996)

$$(\nabla\tau)^2 = C^{-2}(X,Y) = (gD)^{-1}, \tag{5.22}$$

$$\frac{\partial}{\partial s}\left[2C^2\nabla\tau\nabla\eta + \eta C^2\Delta\tau + \eta\nabla\tau\nabla C^2\right] + \Pi\{\eta\} = 0, \tag{5.23}$$

The first Eq. (5.22) is the famous eikonal equation of the ray theory for long waves, allowing the determination of ray paths and wave fronts. This equation may be rewritten in the Hamiltonian form (3.6) (see Chap. 3 and discussion in Sect. 3.1). In the context of rogue waves, it determines the random location of caustics, where the wave field exhibits high amplitudes. The second Eq. (5.23), once integrated, results in

$$2C^2\nabla\tau\nabla\eta + \eta(C^2\Delta\tau + \nabla\tau\nabla C^2) + \frac{3\eta}{D}\frac{\partial\eta}{\partial s} + \frac{D}{3g}\frac{\partial^3\eta}{\partial s^3} = 0. \tag{5.24}$$

Noting that $\nabla\tau\nabla\eta = C^{-1}\ \partial\eta/\partial l$ and calculating $\Delta\tau = b^{-1}d(b/C)/dl$, where l is a coordinate along the ray and b is a distance between neighboring rays, then Eq. (5.24) gives the following equation (see Pelinovsky 1982, Dingemans 1996)

$$C\frac{\partial\eta}{\partial l} + \frac{3\eta}{2D}\frac{\partial\eta}{\partial s} + \frac{D}{6g}\frac{\partial^3\eta}{\partial s^3} + \frac{C\eta}{4Db^2}\frac{d(Db^2)}{dl} = 0. \tag{5.25}$$

This equation stands for the energy flux conservation (3.7) used previously for monochromatic waves in the linear approximation. Equation (5.25) governs the evolution of weakly nonlinear and weakly dispersive waves in a basin with variable depth. The first time, it was derived by Ostrovsky and Pelinovsky (1975). In basins of constant depth (5.25), it reduces to the Korteweg-de Vries equation

$$C\frac{\partial\eta}{\partial X}+\frac{3\eta}{2D}\frac{\partial\eta}{\partial s}+\frac{D}{6g}\frac{\partial^3\eta}{\partial s^3}=0,\quad s=\frac{X}{C}-T, \tag{5.26}$$

$$\frac{\partial\eta}{\partial T}+\frac{3C\eta}{2D}\frac{\partial\eta}{\partial X'}+\frac{CD^2}{6}\frac{\partial^3\eta}{\partial(X')^3}=0,\quad X'=X-CT, \tag{5.27}$$

and describes the evolution of an initial spatial disturbance. The Korteweg-de Vries equation is an etalon equation in the theory of nonlinear waves; it can be solved exactly with the help of the Inverse Scattering Technique (IST) (Novikov et al. 1984, Drazin and Johnson 1989).

When the wave field is directional with significant variation in the transversal direction, then the last term on the LHS of Eq. (5.20) can not be neglected and should be replaced by $\partial(C^2\partial\eta/\partial Y)/\partial Y$, where Y is the transverse coordinate. This term does not allow integration of Eq. (5.23), and the modified evolution equation is now of fourth order, instead of the third order as is Eq. (5.25). In particular, for basins of constant depth, it becomes

$$\frac{\partial}{\partial X'}\left[\frac{\partial\eta}{\partial T}+\frac{3C\eta}{2D}\frac{\partial\eta}{\partial X'}+\frac{CD^2}{6}\frac{\partial^3\eta}{\partial(X')^3}\right]+\frac{C}{2}\frac{\partial^2\eta}{\partial Y^2}=0,\quad X'=X-CT. \tag{5.28}$$

This equation is the famous Kadomtsev–Petviashvili equation that is also completely integrable (Novikov et al. 1984, Drazin and Johnson 1989).

These evolution equations for shallow water waves will be used in the next sections to study the freak-wave phenomenon.

5.2 Nonlinear-Dispersive Focusing of Unidirectional Shallow-Water Wave Fields

Unidirectional shallow water waves are known to be stable with respect to long perturbations. An initial wave field represented by weakly modulated wave trains evolves in time with some change of the shape of the trains, but the waves remain uniform, and their amplitudes do not vary significantly (Kit et al. 2000). Therefore, the modulational instability mechanism that is important for deep water cannot provide wave energy exchange and focusing within a wave group in shallow water. Dispersion, however, still may spawn rogue waves, although the shallow water dispersion law is different from that of deep water. The Korteweg-de Vries (KdV) equation (5.27), derived in the previous section, is a basic weakly dispersive and weakly nonlinear model. This equation was the first that exhibited exact soliton solutions (Zabusky and Kruskal 1965), and the associated Cauchy problem was integrated by using IST (Gardner et al. 1967). The soliton solution is a steady-state solution of Eq. (5.27)

$$\eta(X,T)=H\mathrm{sech}^2\left[\sqrt{\frac{3H}{4D}}\frac{X-VT}{D}\right],\quad V=C\left[1+\frac{H}{2D}\right], \tag{5.29}$$

corresponding to a moving solitary crest on the free surface that was first observed by Scott Russel in a narrow channel in 1844. The soliton length is formally infinite, but physically it is naturally determined at the level of elevation 0.5:

$$\lambda_s = 2D\sqrt{\frac{4D}{3H}}\ln(1+\sqrt{2}) \cong 2D\sqrt{\frac{D}{H}}. \tag{5.30}$$

For instance, a soliton of 1 m height has a length of about 60 km in water of 1 km depth. Solitons are generated from a wide class of initial disturbances that vanish at infinity. Its upper number may be estimated by the formula (Drazin and Johnson 1989)

$$N_s \le 1 + \frac{3}{4D^3}\int\limits_{-\infty}^{\infty} |X|\,(1+\mathrm{sgn}\,(\eta))\,\eta\,(X)\,dX. \tag{5.31}$$

The qualitative character of nonstationary processes of nonlinear wave dynamics within the framework of the Korteweg-de Vries equation can be clarified from the nondimensional form of Eq. (5.27)

$$\frac{\partial\zeta}{\partial t} + \zeta\frac{\partial\zeta}{\partial x} + \frac{1}{9Ur}\frac{\partial^3\zeta}{\partial x^3} = 0, \tag{5.32}$$

where the dimensionless variables $\zeta = \eta/A_0$, $x = X/\lambda_0$, and $t = (3CA_0T)/(2\lambda_0 D)$ are normalized by the amplitude A_0 and length λ_0 of the initial disturbance, respectively. Here, Ur is the Ursell parameter

$$Ur = \frac{A_0\lambda_0^2}{D^3}. \tag{5.33}$$

The physical meaning of the Ursell parameter is evident: it characterizes the ratio of nonlinearity to dispersion. When the Ursell parameter is small, the nonlinearity can be neglected and the wave is a linear dispersive wave. Alternatively, if the Ursell parameter is large, dispersion can be neglected, and the wave evolves as a nonlinear nondispersive wave forming a steep front. For a soliton solution, $Ur = 4$, and this value is marginal, separating nonlinear nondispersive and linear dispersive regimes. This approach and exact solutions will be used in this section to investigate the effect of nonlinear-dispersive focusing.

To study rogue wave generation, it is convenient to invert the time variable in the evolution equation, as similarly done in Chaps. 3 and 4. To do this, the spatial coordinate, X, in the KdV equation should be replaced by $-X$. Hence, an initial value problem for an expected rogue wave may be considered to draw some inferences about wave fields that could form a freak wave (when time is reversed back to its normal run). Vanishing at infinity ($X \to \pm\infty$), boundary conditions result in the simplest analytical analysis of the Cauchy problem.

In particular, solutions for an initial wave in the form of a delta-function (singular initial data) can be obtained analytically (Drazin and Johnson 1989). According

to the exact solution, a positive[1] delta-function evolves into a solitary wave (one soliton) and oscillating dispersive tail. The generated soliton is

$$\eta = \frac{3Q^2}{4D^3}\mathrm{sech}^2\left[\frac{3Q}{4D^3}\left(X - C\left(1+\frac{3Q^2}{8D^4}\right)T\right)\right], \tag{5.34}$$

where Q is the delta-function intensity. The soliton moves with a larger speed and therefore is in front of the wave train; other waves are distributed in space according to the dispersion of the wave velocity. The soliton conserves its shape and energy, while the dispersive tail is spreading in space and thus vanishes. Therefore, the solitary part of the solution is the asymptotic solution of a Cauchy problem for the KdV equation. When the delta function is negative, only a dispersive tail may occur.

Bearing in mind that time may be reversed, this solution actually shows that a delta-function wave may be formed from weak-amplitude waves with or without a soliton. The KdV model does not limit the amplitude of possible abnormal waves; the wave-focusing mechanism due to dispersion is applicable in the nonlinear case as well, but the wave field structure is more complicated and includes amplitude-frequency modulated wave packets and solitons. This process was investigated in detail by Pelinovsky et al. (2000) and Kharif et al. (2000), and is shown in Fig. 5.1 (in the system of coordinates moving with speed C). The value of maximum wave amplitude in the domain increases rapidly and then decreases rapidly again (Fig. 5.2); this explains the short-lived character of rogue waves. Nevertheless, it should be emphasized that the Korteweg-de Vries model is a weakly nonlinear model, and use of singular initial conditions (like delta functions) may be nonphysical. Smoothed bell-like initial conditions with characteristic amplitude, A_0, and length, λ_0, may be considered as well. Negative initial disturbances result in a dispersive tail only; therefore, this process is qualitatively similar to the linear limit (see Sect. 3.2). In this case, the rogue wave is a deep hole on the sea surface (see Fig. 5.3). Positive initial pulse (a crest) may transform into solitons; their number and amplitudes depend on the Ursell parameter (5.33).

When the Ursell parameter is large, the amplitudes of generated solitons are comparable with the amplitude of the initial disturbance (in the limiting case $Ur >> 1$, the amplitude of the leading soliton is two times larger than the initial pulse). Therefore, an initial pulse (that is supposed to be an expected rogue wave) cannot be considered a model of a freak wave, since condition (I.1) for the wave field amplitude amplification is not satisfied.

In the case of a small Ursell parameter, only one soliton is formed with a small amplitude (proportional to Ur). The initial pulse may now be much larger than the wave field at large time, since the soliton amplitude is small, and the dispersive train vanishes. When time is inversed, the evolution may represent a likely process of a rogue wave generation (see Fig. 5.1), while the pulse-like wave may be considered as a freak wave.

[1] This sign depends on the sign of the nonlinear coefficient in the Korteweg-de Vries equation, which is positive for surface water waves.

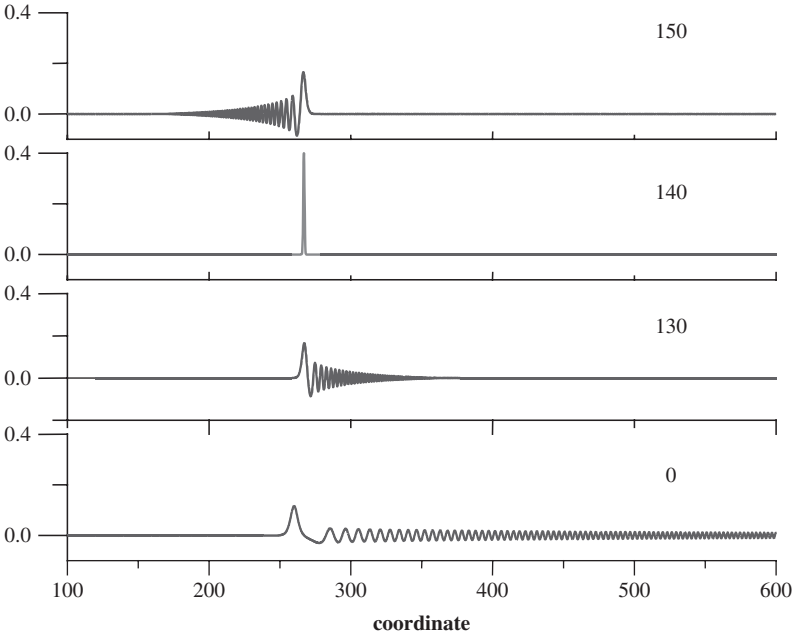

Fig. 5.1 Freak wave formation in shallow water. Numbers denote moments of time (*scaled*)

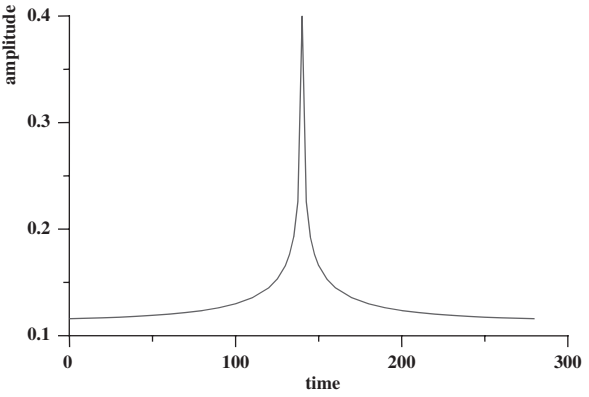

Fig. 5.2 Maximum wave amplitude versus time in the process of the freak wave formation given in Fig. 5.1

It is noteworthy to say that solitons do not play a crucial role in this freak wave generation scenario. The huge wave is mainly due to the frequency-modulated dispersive wave train.

The nonlinear-dispersive mechanism of freak wave formation is relatively robust; weak variation of the wave field parameters modifies the shape and amplitude of the freak wave, but is unable to prevent its occurrence. Specific numerical simulations have been performed in Pelinovsky et al. (2000) and Talipova et al. (2008) to

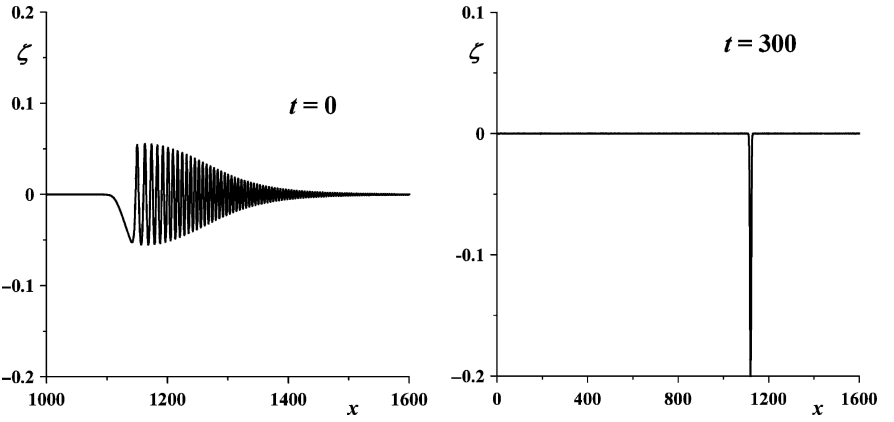

Fig. 5.3 Generation of a deep hole in shallow water

highlight this property. A wave packet generated from a positive narrow pulse (as shown in Fig. 5.1) is inverted in space, $X \to -X$, and then several individual waves are canceled. This wave field is used to start the numerical simulation of the KdV equation. The simulation would result in the initially imposed positive impulse if the wave field has not been cut. If the soliton is deleted from the dispersed wave field (Fig. 5.4a), its focusing results in a freak wave with a large crest and following deep trough (a sign-variable wave; see Fig. 5.4b). If the first negative wave in the train shown in Fig. 5.4a is cut in addition to the soliton wave (Fig. 5.4c), the generated huge wave represents an almost positive pulse (a crest) with no deep neighboring troughs (Fig. 5.4d). The heights of computed abnormal waves in both cases satisfy the amplitude amplification criterion for rogue waves (I.1). Many natural observations support the existence of sign-variable rogue waves (see Chap. 1).

Similar analyses have been performed with a "solitonless" wave train, resulting from a negative pulse disturbance (see Fig. 5.3). If the leading negative oscillation is deleted (see Figs. 5.3a. and 5.5a), the huge wave is represented by several intense waves (Fig. 5.5b) that could be related to the observation of the "three sisters" also presented in Chap. 1.

Besides smooth solutions, singular exact solutions of the Korteweg-de Vries equation may be found (Matveev 2002). Similar to the soliton solutions, they preserve their identity, manifesting elastic collision with other waves. The positon solution is given as an example, although other solutions exist (negaton, singularities, a rational solution; see Matveev 2002)

$$\frac{\eta}{D} = -128p^2 \frac{\sin\Theta(\sin\Theta - p\Psi\cos\Theta)}{(\sin 2\Theta - 2p\Psi)^2}, \tag{5.35}$$

where

$$\Theta = \frac{\sqrt{6}p}{D}\left(X - (1-4p^2)CT\right), \quad \Psi = \frac{\sqrt{6}}{D}\left(X - (1-12p^2)CT\right).$$

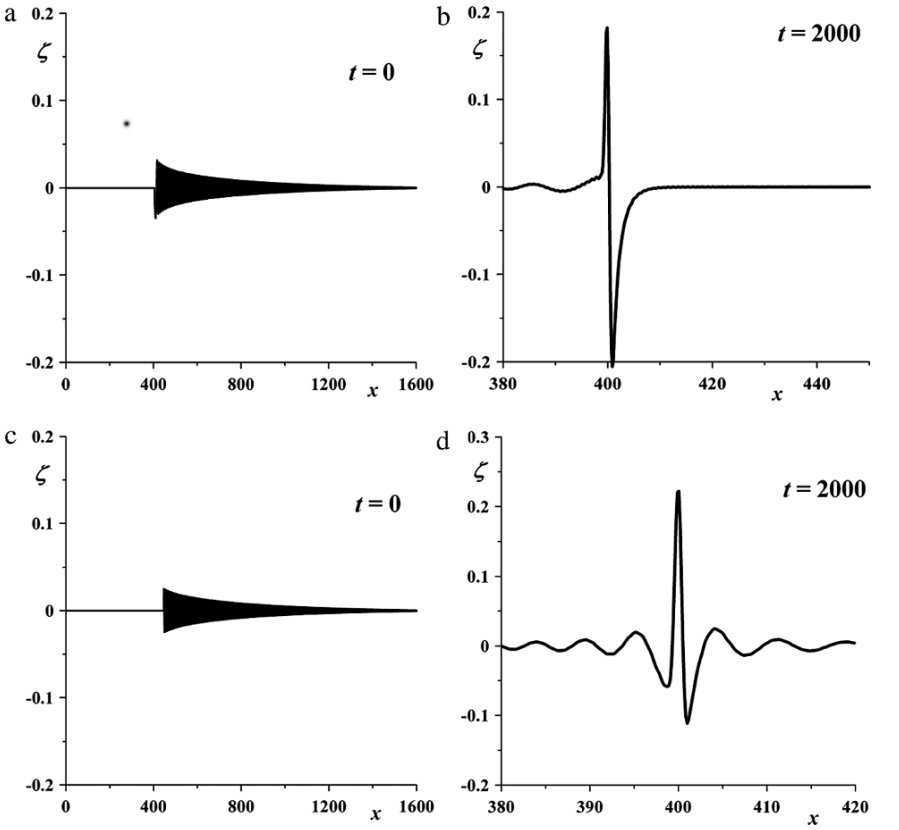

Fig. 5.4 "Non-optimal" focusing of the wave train in shallow water: initial conditions (**a, c**) and resulting waves (**b, d**)

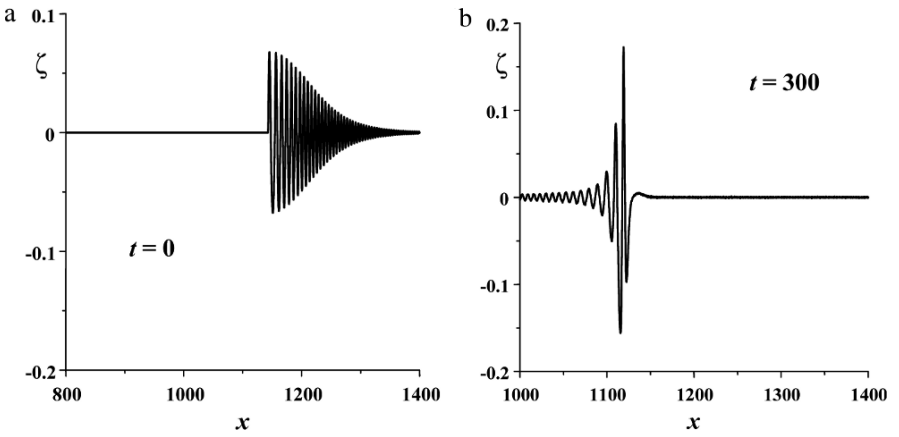

Fig. 5.5 Non-optimal generation of an abnormal wave from the wave train with negative "mass"

The parameter of this solution is p. A positon solution as a function of X has a second-order pole and, therefore, has an infinite energy; the tails of the oscillatory solution. Such solutions cannot be realized physically. They show, moreover, a tendency of smooth solutions of the KdV equation, close to waves with very high peaks.

The solution of the associated scattering problem with periodic boundary conditions is, in fact, much trickier to implement, since it operates with special theta functions. The detailed analysis of periodic solutions of the KdV equation is given in a series of papers by Osborne and coauthors (see, for instance, Osborne 1995, Osborne et al. 1998). The solution of the KdV equation is represented by a linear superposition of nonlinear oscillatory modes (multiple quasi-cnoidal waves) in the associated spectral problem. The freak wave in this approach is the superposition of these modes with suitable phases.

A statistical analysis of shallow-water rogue-wave characteristics has been conducted by Pelinovsky and Sergeeva (2006) with the help of direct numerical simulation of the KdV equation, with periodic boundary and random initial conditions; these results will be discussed in the next section. We would like to emphasize that a superposition of random and weak frequency modulated deterministic components still can efficiently spawn rogue waves, as it is shown in Fig. 5.6 (taken from Pelinovsky et al. 2000). So, freak waves in shallow water may be generated from a wide class of wave fields with the help of the nonlinear dispersive focusing.

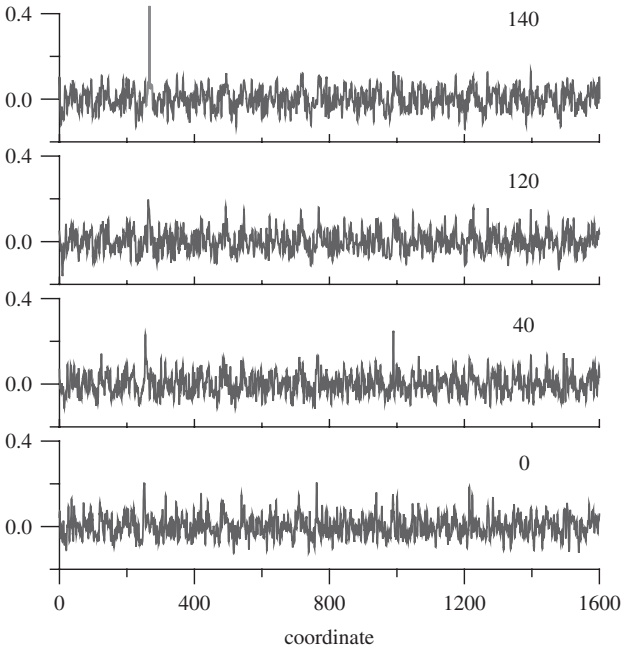

Fig. 5.6 Freak wave formation from the combination of a random field and frequency modulated wave train. Numbers denote moments of time (*scaled*)

5.3 Numerical Modeling of Irregular Wave Fields in Shallow Water (KdV Framework)

In the previous section, it has been shown, with the help of exact and numerical solutions of the KdV equation, how nonlinear-dispersive wave focusing may efficiently generate rogue waves. The KdV equation is integrable with the help of the IST, and this property supports the existence of solitons. When the wave field vanishes as coordinates tend to infinity, solitons are known to represent long-time asymptotic wave behavior, since quasilinear waves decay but solitons remain unchanged.

As shown above in the framework of the KdV equation, the nonlinear dispersive focusing of the wave trains is the major mechanism of freak wave occurrence. The random wave field is characterized by the modulation of the amplitude and frequency of waves. Therefore, the focusing mechanism should "work" in a random field. Meanwhile, the KdV equation is fully integrable, demonstrating an important role of the solitons in nonlinear wave dynamics. For initial disturbances vanishing at infinity, the solitons correspond to the final stage of the wave field evolution, and these results are well known. When the initial disturbance corresponds to the sine periodic wave, its evolution leads to soliton formation and its disappearance (recurrence phenomenon), as has been shown by Zabusky and Kruskal (1965).

Later, this process was investigated for different values of nonlinearity/dispersion ratio (the Ursell parameter given by (5.33)) and large times (see Salupere et al. 2002, 2003a,b and references therein). Actually, an initial sine state is not fully reconstructed at large time, and soliton ensembles play an important role in the long-time behavior of a nonlinear wave field, especially for large values of the Ursell parameter. The dynamics of the soliton ensembles, even for this simple initial sine condition, are very complicated and perhaps may be interpreted as solitonic turbulence, which can be considered as a combination of "rarefied solitonic gas" and the residue of oscillating quasilinear waves (Salupere et al. 1996).

Zakharov (1971) used the inverse scattering method to show that paired collisions occurring between solitons, and the interaction with a nonsoliton field, could not change the amplitude of the soliton. As a result, the total soliton velocity distribution function does not depend on time. In real situations of wind waves, the values of the Ursell parameters are not too large and the dispersive trains contribute significantly to the statistical wave characteristics.

Meanwhile, physically observed wave characteristics (spectra, amplitude, and height distributions) will change. The nonlinear energy exchange between different spectral components even for initial narrow-band wave fields is significant: a wave packet may split into several groups with different carrier wave numbers, and the wave profile becomes asymmetrical (Kit et al. 2000, Grimshaw et al. 2001, Groesen and Westhuis 2002). A wave realization, represented by multicnoidal waves and solitons, varies in space and time more significantly and its behavior is irregular (quasi-chaotic). Moreover, when an initial spectrum has two peaks, such a state is unstable (Zakharov 1971, Onorato et al. 2005), and therefore the wave dynamics should be complicated. As a result, the statistical moments and the distribution functions of the wave field change in time; its spatial spectrum also varies. Under

the assumption of random initial conditions, the properties of such wave fields may be studied with the help of the random functions theory. In fact, we know only one mathematical paper (Murray 1978) where the soliton generation from irregular data is studied, but random wave characteristics have not been considered.

The direct numerical simulation of the KdV equation with periodic boundary conditions is applied in Pelinovsky and Sergeeva (2006) to study the statistical characteristics of wave fields and probability distributions of freak waves. In these simulations, the dimensionless form of the KdV equation (5.32) is used where normalization with significant wave amplitude (for random wave field the significant wave amplitude, A_s, is equal to 2σ, where σ^2 is the variance (2.72)), and carrier wave number K_0 (for random wave field it is the spectral peak wave number) are employed.

The numerical integration of the KdV equation (5.32) with periodic boundary conditions: $\zeta(0,t) = \zeta(L,t)$ is based on a pseudospectral method (Fornberg 1998). A zero-mean random wave field is described by a Fourier series containing 256 harmonics

$$\zeta(x,0) = \sum_{j=1}^{256} \sqrt{2S(k_j)\Delta k}\cos(k_j x + \varphi_j), \tag{5.36}$$

where $S(k)$ is the initial nonsymmetric spectrum, $k_j = j\Delta k$, Δk is the sampling wavenumber, varying from 0.03 to 0.023, and the phase φ_j is a random variable, uniformly distributed in the interval $[0, 2\pi]$. The length of the initial realization is $L = 2\pi/\Delta k$. The initial spectrum is assumed to have a Gaussian shape of amplitude Q, and width δ:

$$S(k) = Q\exp\left(-\frac{(k-1)^2}{2\delta^2}\right). \tag{5.37}$$

The parameter Q is chosen so that $\int_0^\infty 2S(k)\,dk = \sigma_0^2 = 1/4$ (σ_0^2 is the dimensionless variance). The spectral width parameter δ and the Ursell parameter both determine the dynamics of the nonlinear wave field. The sizes of the spectral domain (256 harmonics) and the characteristic spectrum widths are chosen to provide the spectrum decay when k is large. The initial spectra with a cut-off spectrum tail are presented in Fig. 5.7.

In numerical experiments by Pelinovsky and Sergeeva (2006), the Ursell parameter varies from 0.07 to 0.95, and the spectrum width varies from 0.27 to 0.18. Here, only the case $\delta = 0.27$ will be presented in detail. The statistical characteristics are computed for each time step and are averaged over 500 ensembles, which corresponds to a total wave record of about 15,000 individual waves to provide sufficient statistics. The computation is performed for relatively large time evolution, compared with the characteristic time scale of nonlinear effects (till $t = 100$) and includes about 1,000 wave periods depending on the initial conditions. This simulation time is sufficient for the manifestation of nonlinear and dispersive effects and to reach equilibrium conditions.

The evolution of a wave record is displayed in Fig. 5.8 for different instants of time. It is obviously seen that the wave profile becomes asymmetric, so that the

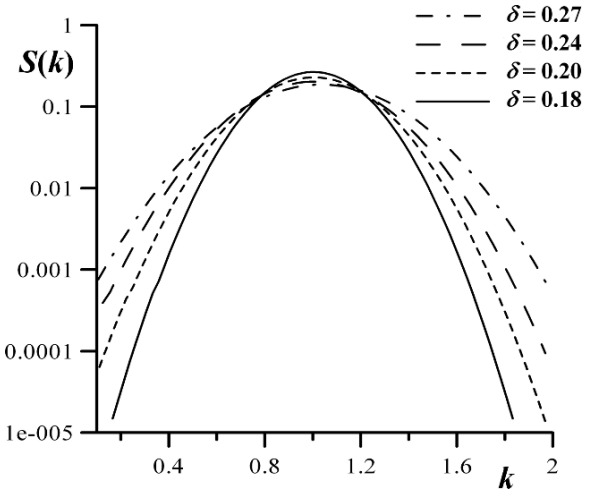

Fig. 5.7 Initial spectra for different widths δ

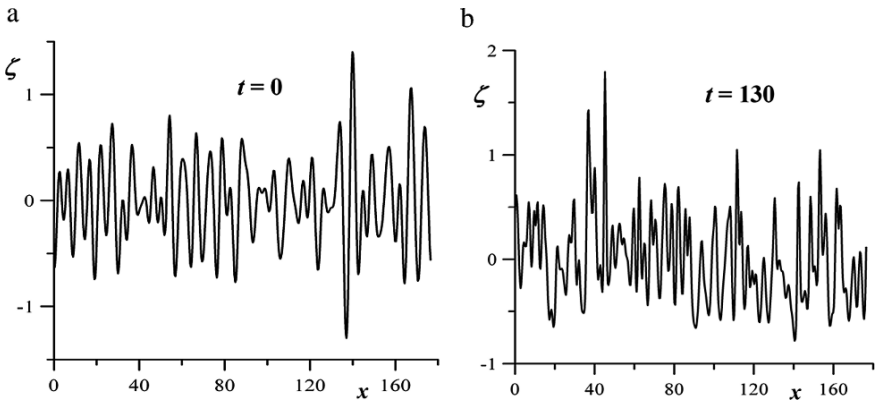

Fig. 5.8 Wave profiles at different instants of time ($Ur = 0.73$)

crests are sharp while the troughs are gentle. It is interesting to analyze the trajectory patterns (Fig. 5.9) presented in the time-space plane. This figure evidently shows solitons' traces for different initial conditions. The number of visible solitons, even for $Ur = 0.95$, is about 5; this means that solitons do not contribute significantly to the total random field. Under conditions of strong nonlinearity, the propagation gives rise to a maximum value of peak amplitude in most realizations (Fig. 5.10a). The key role of nonlinear effects in the formation of large wave amplitudes in this model becomes evident, as shown in Fig. 5.10b. This figure represents the distribution functions of the largest amplitudes, found for the case of numerical simulations and compared with the case of a linear propagation (when the nonlinear term in the KdV equation is canceled). Nonlinearity makes high amplitude wave occurrence more frequent.

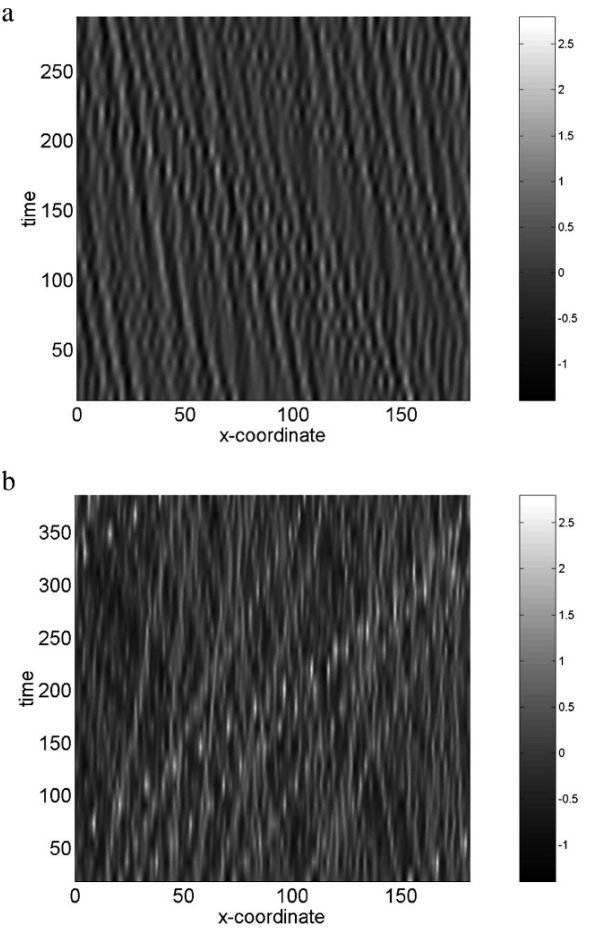

Fig. 5.9 Time-space plane of wave propagation for various Ur. Color gradations show the wave intensity. (**a**) The linear limit $Ur = 0$; (**b**) $Ur = 0.95$

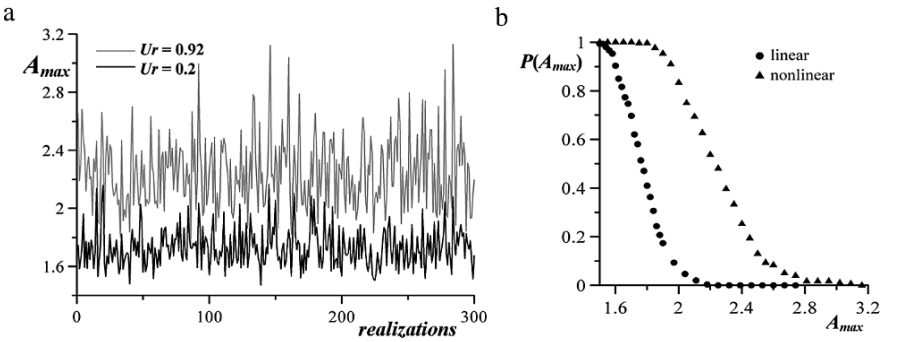

Fig. 5.10 Maximum of wave amplitudes in different realizations (**a**) and distribution of maximum crest amplitudes (**b**)

The first two statistical moments—the mean level and the variance—are integrals of the KdV equation, so that they remain unchanged during the process of wave evolution. The next two statistical moments define the skewness γ and kurtosis

$$\widetilde{\kappa} = \kappa - 3, \tag{5.38}$$

where γ and κ are defined by Eqs. (2.73) and (2.74) (see Chap. 2).

As known, the skewness is a statistical measure of the vertical asymmetry of the wave field. If the value of the skewness increases (positive), the crests are sharper, while the troughs are flatter. The kurtosis represents the degree of peakedness in the distribution and defines the contribution of large amplitude waves in the whole distribution. For a random Gaussian process, $\kappa = 3$, corresponding to $\widetilde{\kappa} = 0$. When $\widetilde{\kappa}$ is positive, the contribution of large waves is more significant. The computed evolution of statistical moments shows a stationary state existence and a transition to this state. The transition period is about 10-20 characteristic time scale of nonlinearity. During this process, both moments of the wave field tend to almost constant values (Fig. 5.11). Figure 5.12 displays the values of γ and $\widetilde{\kappa}$, corresponding to this stationary mode.

For all conditions, the skewness is positive, and it means that the positive waves (crests) have larger amplitudes than the negative waves (troughs). The asymptotic value of skewness increases with an increase of the Ursell parameter; and therefore elevation (positive) waves are more visible in the nonlinear wave field than the depression (negative) waves. This conclusion corresponds to the known expressions for the classical cnoidal waves (sharp crest and flat trough).

The kurtosis tends to a negative asymptotic value for $Ur < 0.6$; therefore, the probability of large amplitude (freak) wave occurrence should be less than is predicted for Gaussian processes. For strong nonlinearity, the kurtosis asymptotic value exceeds zero, which indicates a high probability of large wave occurrence. Onorato

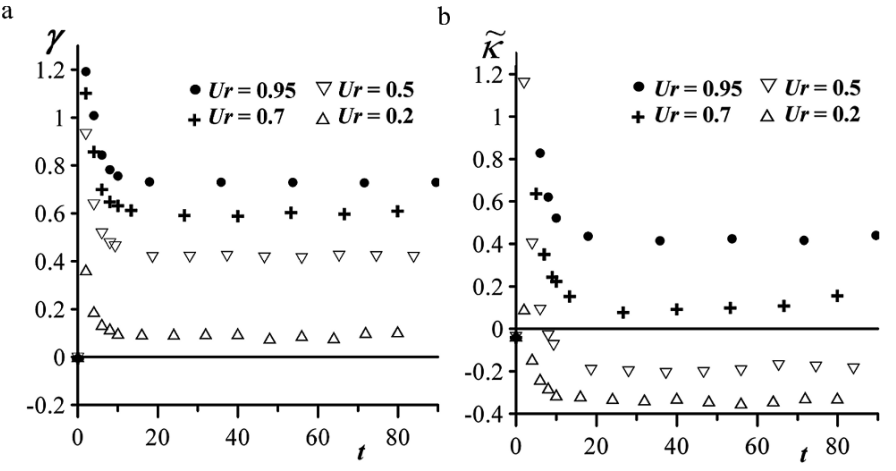

Fig. 5.11 Temporal evolution of statistical moments for different Ursell parameters

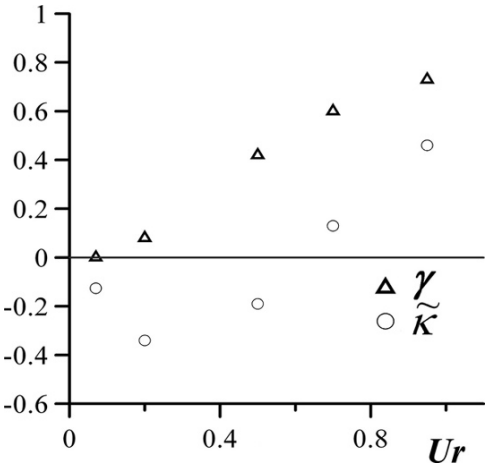

Fig. 5.12 Asymptotic value of the spectral moments as functions of the Ursell parameter Ur

et al. (2001) and Tanaka (2001) showed by means of numerical experiments that for nonlinear random waves over deep water, the kurtosis $\widetilde{\kappa}$ oscillates around some positive mean value. Janssen (2003) reports a positive fourth moment, calculated in the weak turbulence theory for deep-water waves that grow while the wave amplitude increases. Thus, the behavior of the fourth moment is qualitatively similar for strongly nonlinear waves in deep and shallow waters.

As expected due to nonlinearity, the spectrum evolves, widens, and tends to a stationary state (Fig. 5.13). This state, depending on the Ursell parameter, corresponds to the asymmetric wave shape; some energy is transferred to the low frequencies (spectrum downshift phenomenon). For large Ursell values, the spectral density is distributed almost uniformly at small k. The flatness of the spectrum is wider for $Ur = 0.95$ when the wave field is more energetic and nonlinear effects are more significant. The tendency to the flatness of the spectrum (Rayleigh-Jeans spectrum) is known for the statistical equilibrium with no sources and sinks.

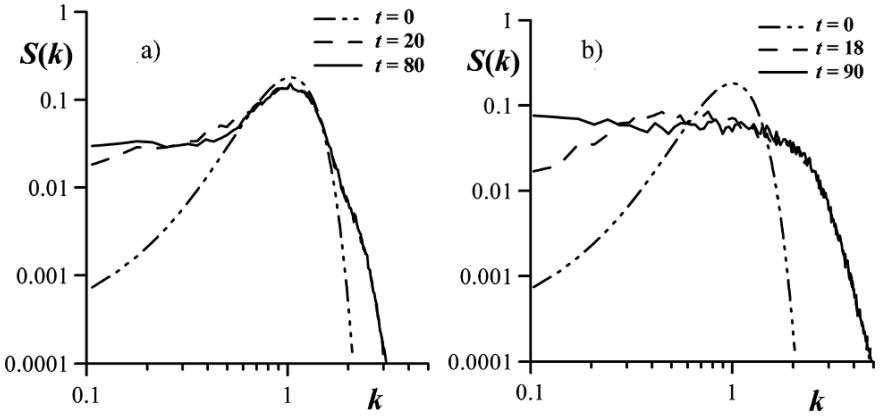

Fig. 5.13 Temporal evolution of spectra $S(k)$ for various Ur: (**a**) $Ur = 0.2$, (**b**) $Ur = 0.95$

It is important to mention that the spectrum downshifts into the low-frequency range even for an initial spectrum taken in a symmetric Gaussian form. For comparison, the downshift of the initial symmetric spectrum for deep-water waves is possible only in the extended version of the nonlinear Schrödinger equation, like the Dysthe equation, which includes an asymmetry of the wave field (Dysthe et al. 2003). The shallow water model based on the KdV equation is initially asymmetric due to the quadratic nonlinearity, and the asymmetry of the wave group is immediately obtained in the process of the wave evolution (Kit et al. 2000, Grimshaw et al. 2001, Groesen and Westhuis 2002). As already noticed, the spectrum becomes asymmetric with weak shifting in the short-wave range. For larger dimensionless wavenumbers $k(0.1 < k < 0.2)$, the spectrum may be approximated by the power law asymptotics $k^{-\alpha}$, where the slope of the spectrum, α, decreases with an increase of the Ur parameter (from $\alpha = 3.7$ for $Ur = 0.5$ till $\alpha = 2$ for $Ur = 0.95$).

The distribution of the wave crest amplitudes, calculated as a maximum between two zero-crossings, is presented in Fig. 5.14. For $Ur < 0.3$, the probability of small amplitudes ($A < 1.2$) exceeds the Rayleigh distribution, which is the theoretical approximation of a linear narrow-band Gaussian process (see Chap. 2); meanwhile, in the range of high amplitudes ($A > 1.5$), the distribution lays below the theoretical curve. For the more energetic wave field ($Ur > 0.3$), the asymptotic distribution exceeds the Rayleigh distribution, and the probability of the highest crest occurrence increases. In a qualitative sense, the shape of the amplitude distribution function does not contradict the behavior of the skewness and kurtosis (Fig. 5.12). The first one shows that positive waves have larger amplitudes than negative waves, whereas the second one indicates a significant contribution of the small waves in the whole distribution. Finally, these results allow us to estimate the probability of the rogue-wave occurrence (its amplitude exceeds twice the significant amplitude; see (I.1)). Freak waves should appear more frequently when the wave field is strongly nonlinear (high values of the Ursell parameter).

The same results are obtained when using experimental spectra of shallow-water waves in the coastal zone of the North Sea and in Lake Georgia in Australia

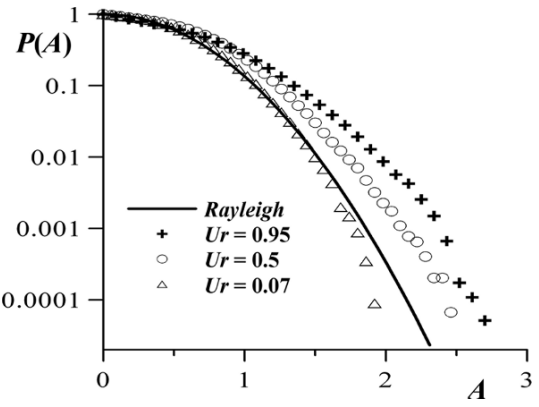

Fig. 5.14 Asymptotic crest amplitude distribution for different Ur numbers. *Solid line* corresponds to the Rayleigh distribution

(Kokorina and Pelinovsky 2005). The computed results confirm that the irregular nonlinear wave field does not satisfy the Gaussian statistics, and its statistical characteristics depend on the Ursell parameter, which represents the "ratio" of nonlinear to dispersive effects.

In this way, it is demonstrated that the nonlinear shallow water-wave field becomes asymmetric with sharp crests and flat troughs, which leads to a positive third statistical moment. The skewness grows monotonously with the increase of the Ur number. The behavior of the 4th statistical moment (kurtosis $\widetilde{\kappa}$) is nonmonotonic. It is negative when $Ur < 0.8$, which indicates a significant contribution of small amplitude waves to the total distribution. When the initial disturbance is more nonlinear, then the kurtosis exceeds the zero level, at which it increases with a growth of Ur. For small Ur numbers, close to zero, the probability distribution function slightly deviates from the theoretical Rayleigh distribution. For $Ur > 0.3$, the computed curve lies above the theoretical distribution, which means a higher probability of large wave formation—namely freak-wave occurrence. An important result is the existence of a steady state for statistical characteristics: statistical moments (skewness and kurtosis), distribution functions, and spectral density. The computations demonstrate that both the statistical moments and distribution functions evolve until some bound level is reached. The analysis of a random wave-spectrum evolution shows the same effect. The initially symmetric power spectrum with a Gaussian shape broadens with time, and energy is transferred down the spectrum. For a period of time approximately equal to 20 of a characteristic time scale of nonlinearity, the spectrum relaxes to some stationary state with energy concentration in the low frequency range, as has been already noticed. The parameters of the equation—in particular the Ur parameter—influence the width of the steady spectrum. For strong nonlinearity, the established stable spectrum is wider, and the energy is distributed almost uniformly in the range of long waves.

5.4 Three-Dimensional Rogue Waves in Shallow Water

When two horizontal coordinates are considered, rogue waves can appear owing to (i) the focusing of transient wave groups, and (ii) spatial (geometric) focusing of water waves. Nonlinear models of spatially inhomogeneous wave fields are complex even in basins of constant depth. They have been used to model freak-wave occurrence in 3D transient trains. Qualitatively, nonlinear processes support linear mechanisms of huge wave formation (see references in Sect. 3.2).

To clarify new, essentially nonlinear effects occurring in spatial inhomogeneous wave fields, let us first consider the interaction of two oblique propagating solitary waves. Basic equations for weakly nonlinear and weakly dispersive water waves were discussed in Sect. 5.1. It is convenient here to rederive such equations for the "equivalent" potential, q (it corresponds to the dimensional first term in the series (5.6), q_1) and dimensionless water displacement, ζ (Miles 1977a,b, Pelinovsky 1996)

$$\zeta = -\frac{\partial q}{\partial t} - \frac{\alpha}{2}(\nabla q)^2 + \frac{\beta}{2}\frac{\partial^3 q}{\partial t^3}, \tag{5.39}$$

$$\frac{\partial^2 q}{\partial t^2} - \Delta q = -\alpha \frac{\partial}{\partial t}\left[\frac{1}{2}\left(\frac{\partial q}{\partial t}\right)^2 + (\nabla q)^2\right] + \frac{\beta}{3}\frac{\partial^4 q}{\partial t^4}, \tag{5.40}$$

where coordinates are normalized with the wave length, λ, time, with the wave period, displacement, and with the wave amplitude, A. As a result, two parameters—$\alpha = A/D$ and $\beta = (D/\lambda)^2$—characterize the weak nonlinearity and dispersion, respectively. When two solitons propagate in different directions, it is convenient to make a change of coordinates as follows:

$$\xi_1 = y\cos\Psi_1 + x\sin\Psi_1 - t, \quad \xi_2 = y\cos\Psi_2 + x\sin\Psi_2 - t, \quad \tau = \alpha t. \tag{5.41}$$

In these new variables, Eqs. (5.39) and (5.40) become

$$\zeta = (\partial_1 + \partial_2 - \alpha\partial_\tau)q - \alpha\left[\frac{(\partial_1 q)^2 + (\partial_2 q)^2}{2} + (1-2\theta)\partial_1 q\partial_2 q\right] - \frac{\beta}{2}(\partial_1 + \partial_2)^2 q, \tag{5.42}$$

$$\alpha(\partial_1 + \partial_2)\left\{2\partial_\tau q + \left[\frac{3}{2}(\partial_1 q)^2 + \frac{3}{2}(\partial_2 q)^2 + (3-4\theta)\partial_1 q\partial_2 q\right]\right\} + \frac{\beta(\partial_1 + \partial_2)^3 q}{3} - 4\theta\partial_1\partial_2 q = 0, \tag{5.43}$$

where $\theta = \sin^2[(\Psi_1 - \Psi_2)/2]$ corresponds to the difference in the soliton propagation directions; ∂_1 and ∂_2 denote derivation with respect to coordinate ξ_1 and ξ_2, respectively. In particular, the case $\Psi_1 = 90^\circ$ and $\Psi_2 = -90^\circ$ corresponds to the counter propagation of solitary waves. The solution of Eq. (5.43), to the first order of the nonlinear parameter (assuming $\alpha \sim \beta$), can be sought as

$$q = F_1(\xi_1, \tau) + F_2(\xi_2, \tau) + \alpha F_{12}(\xi_1, \xi_2, \tau). \tag{5.44}$$

Here, $\partial F_{1,2}/\partial\xi_{1,2}$ (it is proportional to the water displacement in the linear theory of long waves) are the "non-interacting" solitons described by the unidirectional KdV equation

$$2\alpha\frac{\partial F_{1,2}}{\partial\tau} + \frac{3\alpha}{2}\left(\frac{\partial F_{1,2}}{\partial\xi_{1,2}}\right)^2 + \frac{\beta}{3}\frac{\partial^3 F_{1,2}}{\partial\xi_{1,2}^3} = 0. \tag{5.45}$$

After substitution of Eq. (5.44) in Eq. (5.43), and taking into account Eq. (5.45), the first nonlinear correction to the potential is expressed by

$$F_{12}(\xi_1, \xi_2, \tau) = \frac{3-4\theta}{4\theta}\left(\frac{\partial}{\partial\xi_1} + \frac{\partial}{\partial\xi_2}\right)F_1(\xi_1, \tau)F_2(\xi_2, \tau). \tag{5.46}$$

As a result, the series (5.44) can be written with the same accuracy as Miles (1977a,b)

$$q = F_1(\xi_1 + \rho_2, \tau) + F_2(\xi_2 + \rho_1, \tau), \tag{5.47}$$

where

$$\rho_{1,2} = \alpha\left(\left(\frac{3}{4\theta} - 1\right) F_{1,2}(\xi_{1,2}, \tau)\right). \tag{5.48}$$

Similarly, the water displacement at the first order of nonlinearity is given by

$$\zeta = N_1(\xi_1 + \rho_2, \tau) + N_2(\xi_2 + \rho_1, \tau) + \alpha I N_1 N_2, \tag{5.49}$$

$$N_i = \left(\frac{\partial}{\partial \xi_i} - \frac{\beta}{3}\frac{\partial^3}{\partial \xi_i^3}\right) F_i + \frac{\alpha}{4}\left(\frac{\partial F_i}{\partial \xi_i}\right)^2, \quad I = \frac{3}{2\theta} - 3 + 2\theta. \tag{5.50}$$

The result of the interaction of two solitons depends on the angle between the soliton directions (expressed by the parameter θ). The coefficient of the interaction is $I = 0.5$ for solitons propagating toward each other ($\Psi_1 - \Psi_2 = 180^\circ$), then it weakly decreases (down to 0.464) when $\Psi_1 - \Psi_2$ decreases to 138°, and then grows to infinity when the waves copropagate.

The breakdown of the perturbation technique for waves propagating in almost the same directions is evident from the mathematical point of view, because the two new coordinates, ξ_1 and ξ_2, are not independent in this case. From a physical point of view, almost parallel propagation of two solitons leads to strong interaction between them, and each soliton changes the trajectory of the propagation of the other soliton. In the vicinity of the almost parallel wave propagation, the solution should be obtained directly from the nonlinear evolution equations: the Kadomtsev-Petviashvili equation if the waves propagate almost parallel, or the KdV equation if the waves propagate in one direction.

The Kadomtsev-Petviashvili equation was derived in Sect. 5.1 and is reproduced here in dimensionless form

$$\frac{\partial}{\partial x}\left(\frac{\partial \zeta}{\partial t} + 6\zeta\frac{\partial \zeta}{\partial x} + \frac{\partial^3 \zeta}{\partial x^3}\right) = -3\frac{\partial^2 \zeta}{\partial y^2}, \tag{5.51}$$

where $\zeta = 3\eta/2D$, $x = X/D$, $y = Y/D$ and $t = CT/6D$. The Kadomtsev-Petviashvili equation is also integrable (Drazin and Johnson 1989) and therefore exact solutions can be used to study the soliton interaction. It is convenient to use the Hirota transformation

$$\zeta = 2\frac{\partial^2}{\partial x^2}\ln\Gamma(x, y, t), \tag{5.52}$$

to reduce Eq. (5.51) to bilinear form

$$\Gamma\left(\frac{\partial^2 \Gamma}{\partial t \partial x} + \frac{\partial^4 \Gamma}{\partial x^4} + 3\frac{\partial^2 \Gamma}{\partial y^2}\right) - \frac{\partial \Gamma}{\partial t}\frac{\partial \Gamma}{\partial x} - 3\left(\frac{\partial \Gamma}{\partial y}\right)^2 - 4\frac{\partial \Gamma}{\partial x}\frac{\partial^3 \Gamma}{\partial x^3} + 3\left(\frac{\partial^2 \Gamma}{\partial x^2}\right)^2 = 0. \tag{5.53}$$

The plane soliton of the Kadomtsev-Petviashvili equation

$$\zeta = \frac{k^2}{2}\mathrm{sech}^2(k\xi/2), \quad \xi = k(x - py - Vt), \quad V = k^2 + 3p^2 \tag{5.54}$$

in the framework of Eq. (5.53) is expressed in the simple form

$$\Gamma = 1 + \exp(\xi). \tag{5.55}$$

Here, p determines the slope of the soliton trajectory in space. Similarly, the two-soliton solution of Eq. (5.53) can be written explicitly (Satsuma 1976):

$$\Gamma = 1 + \exp(\xi_1) + \exp(\xi_2) + r^2 \exp(\xi_1 + \xi_2), \tag{5.56}$$

$$\xi_i = k_i(x - p_i y - V_i t), \qquad r^2 = \frac{(k_1 + k_2)^2 + (p_1 + p_2)^2}{(k_1 - k_2)^2 - (p_1 + p_2)^2}.$$

Solitons are separated in space except the area of interaction around the moving point:

$$x^* = \frac{V_1 p_2 - V_2 p_1}{p_2 - p_1} t, \qquad y^* = \frac{V_1 - V_2}{p_2 - p_1} t. \tag{5.57}$$

The shapes of the large-amplitude waves occurring in the process of the two-soliton interaction for various angles between soliton fronts are given in Fig. 5.15 from the paper by Peterson et al. (2003). The wave amplitude depends strongly on the angle between the soliton fronts. Similar combinations of nonlinearly interacting waves may be often observed in nature near the coast (see Fig. 5.16).

To show the main features of the oblique interaction of solitons and calculate possible parameters of the enhanced wave, let us consider two solitons with the same amplitudes ($k_1 = k_2$) traveling symmetrically with respect to the Ox axis ($p_1 = -p_2$). As often used in wave physics, such an interaction is equivalent to the wave reflection at the wall located at $y = 0$. Then the condition $p_1 = -p_2$ has the meaning of

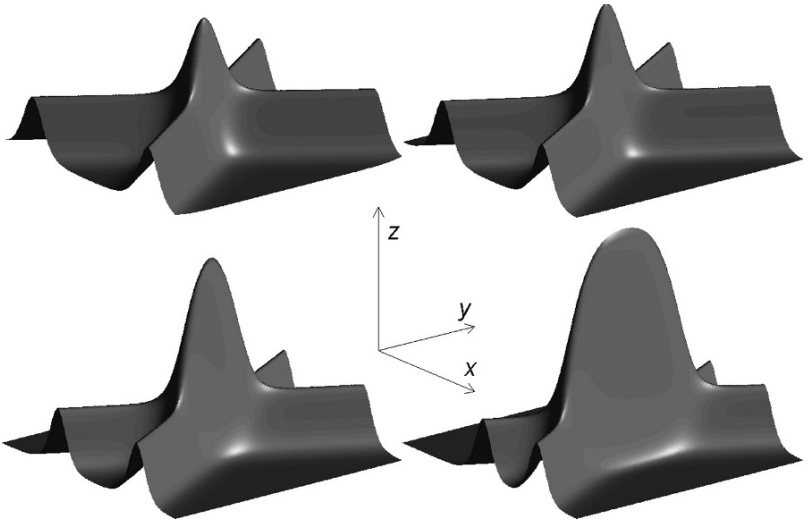

Fig. 5.15 Large-amplitude waves occurring in the process of soliton interaction. Reproduced from (Peterson et al. 2003) by permission of European Geosciences Union

Fig. 5.16 Crescent nonlinear wave trains near the shore. A growing breaking wave is readily observed (Courtesy of I.I. Didenkulova)

the well-known Snell law (the reflection angle is equal to the incident angle). Such a situation with oblique soliton reflection is very often reproduced in laboratories (Melville 1980, Funakoshi 1980, Mase et al. 2002). In this case, the solitons propagate with the same speed ($V_1 = V_2$) and the pattern of wave interaction is stationary, while the interacting area moves along the Ox axis with constant speed. Under these conditions, the wave field is expressed as

$$\zeta(x,y,t) = 2k^2 \frac{1 + r\cosh[k(x-Vt)]\cosh(kpy)}{\{\cosh[k(x-Vt)] + r\cosh(kpy)\}^2}, \quad r = \sqrt{1 - \left(\frac{k}{p}\right)^2}. \tag{5.58}$$

The water displacement on the wall ($y = 0$) can be found from Eq. (5.58); and in dimensional variables it reads

$$\frac{H_w}{H_0} = \frac{4}{1 + \sqrt{1 - \dfrac{3H_0}{D\tan^2\Theta}}}, \tag{5.59}$$

where H_0 is the height of the incident soliton, and Θ is the angle between the soliton front and the Oy axis (see sketch in Fig. 5.17a).

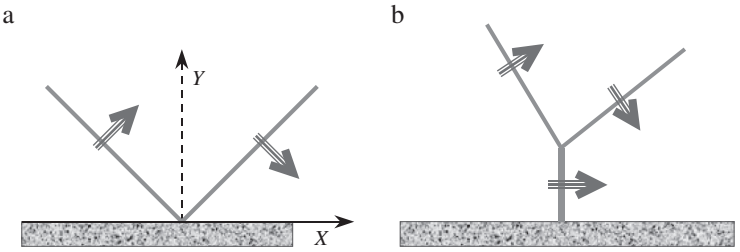

Fig. 5.17 Soliton reflection from a wall: quasi-linear reflection (**a**) and Mach stem formation (**b**)

At $\Theta \sim \pi/2$ (normal approach of the wave to the wall or, alternatively, counter soliton propagation), the wave height is increased almost twice and the same result can be obtained from the perturbation analysis (5.49). At small angles ($\tan^2\Theta \sim 3H_0/\mathrm{D}$), when the soliton propagates almost along the wall, the wave amplification near the wall can reach the value of four, and this is the result of joint action of nonlinear and diffraction effects that are of the same order of magnitude. But when the angle is very small ($k > p$), the solution (5.58) becomes complex and cannot describe the physical wave field. This means that wave fields at small angles are not stationary, and the interaction area should "take off" from the wall. In fact, this can be achieved from (5.58). When the solitons propagate toward each other with almost parallel wave crests, the incident and reflected solitons are well-separated everywhere in space (Fig. 5.17a). When $p \to k$, the induced soliton appears near the wall and propagates along the wall (Fig. 5.17b). The amplitude of this wave (5.59) and its speed (5.57) are different from those of a Korteweg-de Vries soliton, and it can be called a "virtual" soliton (Onkuma and Wadati 1983). Only under special conditions can this wave become a true soliton and propagate along the wall (the so-called Mach stem). Let us assume that the parameters of the incident (i) and reflected (r) solitons are related as

$$k_i + k_r = p_i + p_r. \tag{5.60}$$

Thus, $r = 0$ and the two-soliton solution (5.56) is

$$\Gamma = 1 + \exp(\xi_i) + \exp(\xi_r). \tag{5.61}$$

The wave (the Mach stem) propagates along the wall ($y = 0$) if

$$k_i p_i = k_r p_r, \tag{5.62}$$

which is the Snell law for wave reflection. Parameters of the reflected soliton may be found explicitly from Eq. (5.60) to Eq. (5.62)

$$k_r = p_i, \quad p_r = k_i > p_i, \tag{5.63}$$

and soliton speeds are not equal: $V_r < V_i$. It confirms that the process of wave reflection is not stationary and can be interpreted as a resonant interaction of three solitons: incident, reflected, and the Mach stem. The wave height at the wall can be found in Eq. (5.61), and in dimensional form it reads

$$\frac{H_w}{H_0} = \left[1 + \frac{\tan\Theta}{(3H_0/D)^2}\right]^2. \tag{5.64}$$

Formulas (5.59) and (5.64) describe the nonmonotonic character of the wave amplification. Its maximum (four) is achieved when the angle between waves is of the same order as the nonlinear parameter A/D. Formation of the Mach stem

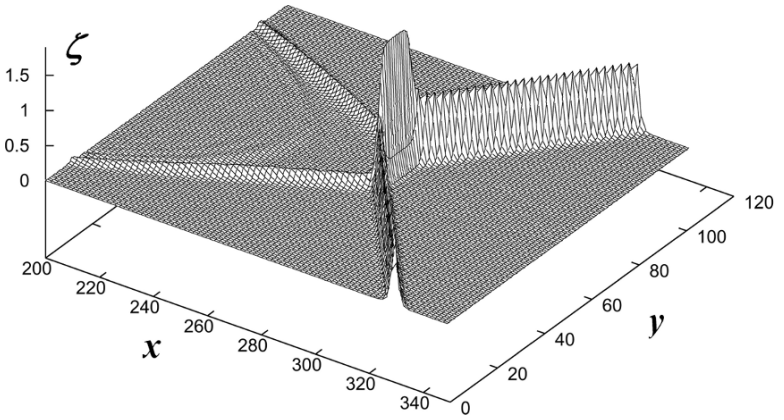

Fig. 5.18 Formation of the Mach stem in almost collinear soliton interaction. Reproduced from Porubov et al. (2005) with permission from Elsevier

was studied numerically by Porubov et al. (2005); Fig. 5.18 illustrates this process in the general case. The wave steepness in the process of two-soliton interactions can be enhanced to a value eight times that of the initial steepness (Soomere and Engelbrecht 2005).

It is important to note that two-soliton interaction leads to the formation of a rogue wave with an infinite lifetime. Specific numerical simulations of the Cauchy problem for the Kadomtsev-Petviashvili equation performed in Porubov et al. (2005) show that the result of the interaction of initially separated solitons depends strongly on the curvature of the initial fronts, and the maximum amplification in the interacting area can be very large. In fact, a combination of two different effects takes place in this case: nonlinear interaction of solitons and geometrical focusing. The same effect may be observed at random wave incidence (Mase et al. 2002). Figure 5.19 shows the effect of the Mach stem formation in a laboratory tank.

So, comparison with unidirectional wave-field dynamics in shallow water shows that soliton interactions play a significant role in localized rogue wave formation. Toffoli et al. (2006) performed detailed calculations of the statistical properties of shallow water waves in crossing seas within the framework of the Kadomtsev-Petviashvili equation. Numerical simulations indicate that the interaction of two noncollinear wave trains generates steep and high amplitude peaks, thus enhancing the deviation of the surface elevation from the Gaussian statistics. These peaks yield a modification of the upper tail of the probability density function for surface elevation, which significantly deviates from the distribution of wave elevation in the unimodal condition. The coexistence of two spectral peaks, therefore, enhances the nonlinearity of the wave field, which results in an increase of the skewness and kurtosis. Whereas this enhancement is negligible for nearly collinear waves, the skewness and kurtosis reach high values when the two spectral peaks have well-separated directions.

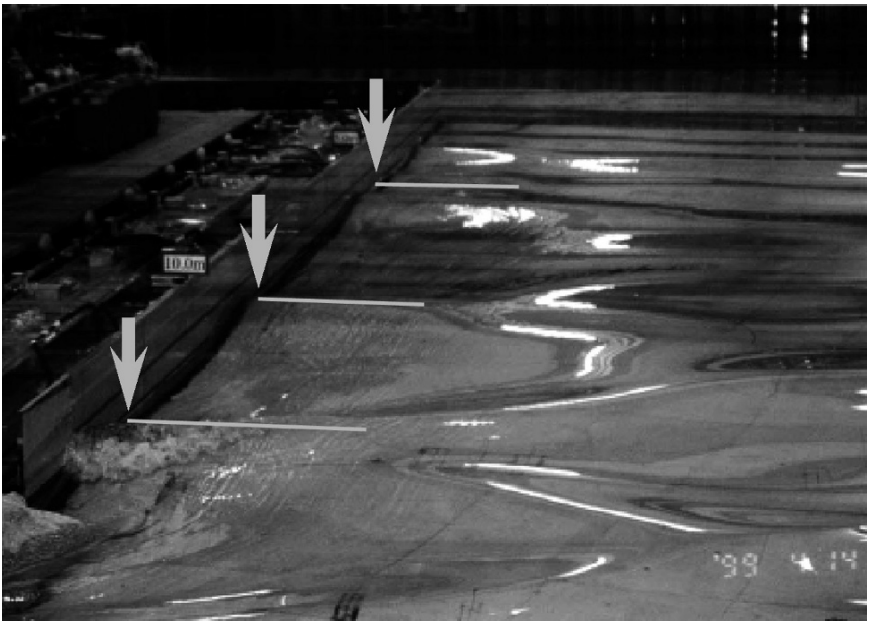

Fig. 5.19 Formation of Mach stem (see arrows) near the vertical wall at random wave incidence. Reproduced from (Mase et al. 2002) with permission from Elsevier

5.5 Anomalous High Waves on a Beach

The rogue wave phenomenon is usually discussed in terms of waves in seas and oceans far from the shores. Such unusual waves are observed also in the coastal zone and on coastlines. Excellent photos of freak waves on rocky coasts are given in Chap. 1 (Fig. 1.1h), when a freak wave reached height of 25 m approximately 4 sec after it became visible near the coast of Vancouver Island, Canada. Other freak waves attacked the breakwater in Kalk Bay (South Africa) on April 21, 1996 and August 26, 2005. In both events, the freak wave washed off the breakwater people, some of whom were injured. The freak waves induced panic at Maracas Beach (Trinidad Island, Lesser Antilles) on October 16, 2005, when a series of towering waves, many more than 25 feet high (height of 8 m), flooded the beach, forcing sea-bathers, venders, and lifeguards to run for their lives (see Fig. 1.1g).

The wave field in coastal zones contains strong coherent components and may be represented as the nonlinear superposition of solitary (solitons), cnoidal, and breaking waves (undular and smooth bores). Their interaction can generate narrow "spots" of large-amplitude freak waves. The bottom topography plays a significant role in spatial (geometric) interference of waves, resulting in the formation of random focusing and caustic points, where the wave field is amplified. The effect of water wave amplification in the coastal zone is well known. It means that probability of large-amplitude waves should increase in the coastal zone. In this section, we

will investigate the probability of freak waves on the background of high-amplitude coastal waves (tails of the probability distribution function).

5.5.1 Waves at Vertical Walls

First, one of the typical nonlinear effects in the coastal zone will be considered and analyzed when the wave propagates close to vertical walls (rocks, breakwaters, other vertical structures) and may suffer reflection. A simplified geometry of the coastal zone is shown in Fig. 5.20. The wave approaches the vertical wall located at $X = 0$ from the left. For the sake of simplicity, the incident wave is represented as a single crest, but later we will consider the incident wave as a continuous function, describing random crests and troughs. The basic equations for water waves in shallow water are

$$\frac{\partial \eta}{\partial T} + \frac{\partial}{\partial X}\left[(D+\eta)\,u\right] = 0, \qquad \frac{\partial u}{\partial T} + u\frac{\partial u}{\partial X} + g\frac{\partial \eta}{\partial X} = 0, \tag{5.65}$$

where $u(X,T)$ is the depth-averaged horizontal velocity of the water flow (see Eq. (5.10)) and $\eta(X,T)$ is the vertical displacement of the sea level.

The boundary condition on the vertical wall corresponds to the total reflection of the wave energy and no penetration of fluid through the wall is considered:

$$u(X = 0, T) = 0. \tag{5.66}$$

Another condition that concerns the approach of the incident wave to the wall from the left will be discussed. To solve Eq. (5.65), it is convenient to introduce the Riemann invariants

$$I_{\pm} = u \pm 2\left[\sqrt{g(D+\eta)} - \sqrt{gD}\right], \tag{5.67}$$

and rewrite system (5.65) in the following form

$$\frac{\partial I_{\pm}}{\partial T} + C_{\pm}\frac{\partial I_{\pm}}{\partial X} = 0, \tag{5.68}$$

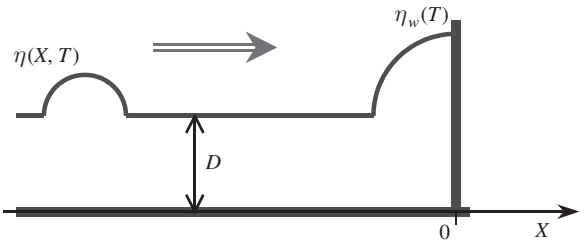

Fig. 5.20 Definition sketch of the considered geometry

where the characteristic speeds are

$$C_{\pm} = \pm\sqrt{gD} + \frac{3}{4}I_{\pm} + \frac{1}{4}I_{\mp}. \tag{5.69}$$

According to Eq. (5.68) each invariant remains constant along the characteristic curves

$$\frac{dI_{\pm}}{dT} = 0 \quad \text{along} \quad \frac{dX}{dT} = C_{\pm}. \tag{5.70}$$

Note that the characteristic speeds depend on both invariants, and nonlinearity bends the characteristics in the vicinity of the wall area where the incident and reflected waves interact. When taking into account conservation of the Riemann invariants, the effect of wave interaction yields phase corrections of the travel times of different parts of the wave profile. As a result, the water displacement at the vertical wall $\eta_w(T) = \eta(X = 0, T)$ depends on the incident wave in a very complicated manner, and cannot be found in an explicit form. Nevertheless, the relation between values of the wave in the incident field and in the near-wall water oscillations can be derived explicitly. Outside the interaction near-wall area, the incident and reflected waves propagate independently. The incident wave is characterized by

$$I_{-} = 0, \quad u = 2\left[\sqrt{g(D+\eta)} - \sqrt{gD}\right], \quad I_{+} = 4\left[\sqrt{g(D+\eta)} - \sqrt{gD}\right]. \tag{5.71}$$

Due to the boundary condition (5.66), the incident invariant at the wall is

$$I_{+} = 2\left[\sqrt{g(D+\eta_w)} - \sqrt{gD}\right]. \tag{5.72}$$

From the conservation of I_{+} along the characteristic curves it follows that

$$\frac{\eta_w(T)}{D} = 4\left[1 + \frac{\eta(T-\tau)}{D} - \sqrt{1 + \frac{\eta(T-\tau)}{D}}\right]. \tag{5.73}$$

So, the water level on the wall can be expressed through the water displacement of the incident wave. Unfortunately, this method cannot predict the time-lag, τ, which is generally an unknown functional of the wave field in the interaction zone. This is why expression (5.73) cannot be straightforwardly applied for calculations of the water level oscillations near the vertical wall, even when all the characteristics of the incident wave are known. However, a practical formula can be derived from (5.73)—it is the relation between the extreme values of the wave field

$$\frac{R}{D} = 4\left[1 + \frac{A}{D} - \sqrt{1 + \frac{A}{D}}\right], \tag{5.74}$$

where A is the positive or negative amplitude (crest or trough height) of the incident wave, and R is the amplitude of water level oscillations on the wall. This relation is plotted in Fig. 5.21 (solid line).

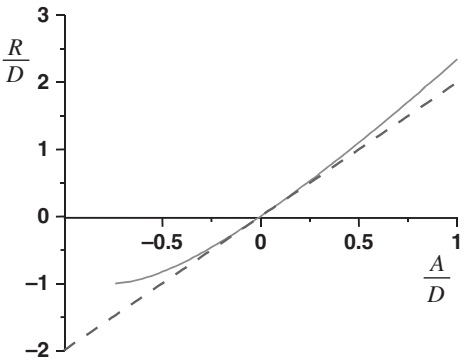

Fig. 5.21 Amplitude of water oscillations at the wall (R) versus the incident wave amplitude (A) according to the linear (*dashed*) and nonlinear (*solid*) theories

The linear limit gives the following relation between the wave characteristics, $R = 2A$. This curve is plotted by dashed line in Fig. 5.21 for comparison. As can be seen, the nonlinearity increases the crest height and decreases the trough height at the wall. In fact, the weak increase of the wave height, when the positive wave (crest) comes near the wall, was analyzed earlier by Mirchina and Pelinovsky (1984) and Pelinovsky and Mazova (1992). A more interesting case occurs when the negative wave (trough) comes near the wall. The nonlinear effects become stronger when the total depth tends to zero. The algebraic solution (5.74) exists only if the trough amplitude is less than $3D/4$; in other words, if the total depth under the trough is greater than $D/4$.

The process of the wave interaction with a vertical wall has been considered for a pulse-like shape of a certain polarity, but this restriction is actually unnecessary. The expression (5.74) can be obtained for an arbitrary function $\eta(T)$, finite or continuous in time, if its shape is sufficiently smooth. The conditions of application of the derived relation between the amplitude of the water oscillations at the wall and the incident wave amplitude are discussed in Pelinovsky et al. (2008). It is shown that the analytical expression (5.74) is valid at least for smooth incident waves if the crest amplitude is less than $3D$ and the trough amplitude is less than $5D/9$. These criteria are obtained from the shallow-water theory, which does not include wave dispersion. Within the framework of the nonlinear-dispersive theory, the height of steady-state waves (cnoidal or solitary waves) is limited as $H = 2A < 0.78D$. According to many laboratory data, where the role of dispersion is important, the wave height is bounded by $0.55D$ (see Massel 1996b). Further, we will use the closed criterion for the normalized significant wave height/depth, $H_s/D < 0.5 \div 0.7$.

The approach applied above is valid for any incident wave that is regular, as well as irregular, due to the wave separation along characteristics. In the latter case, it can be used to analyze distribution functions of the wave field and its spectrum. Unfortunately, it cannot predict the time-lag between the incident wave and water oscillations at the wall, and therefore the function $\eta_w(\tau)$ is not fully determined within the framework of the nonlinear theory. The process is not Gaussian due to nonlinearity, and all the moments cannot be calculated, including the significant height of water oscillations at the wall. On the other hand, the relationship between

random wave amplitudes of the incident wave and water oscillations at the wall (see Eq. (5.74)) is explicit and does not include the time-lag. Hence, as soon as the distribution function of the wave amplitude of the incident wave field is known, expression (5.74) can be used to obtain the distribution function of the amplitude of the water oscillations at the wall. The noninertial ("instant") transformation of random processes is described in various books (see Massel 1996a). The exceedance probability function of the water oscillation amplitude at the wall can be determined as follows

$$P_R(R) = P_A(A)|_{A(R)}\,, \tag{5.75}$$

where $A(R)$ is the inverse function obtained from Eq. (5.74), which is known explicitly as

$$\frac{A}{D} = \frac{R}{4D} + \frac{1}{2}\left[\sqrt{1+\frac{R}{D}} - 1\right]. \tag{5.76}$$

For detailed calculations, the exceedance probability function of the incident wave should be specified. Below, the Rayleigh distribution for wave heights is used (indices of distribution functions will be omitted in the following formulas)

$$P(H) = \exp\left(-\frac{H^2}{8\sigma^2}\right) \approx \exp\left(-\frac{2H^2}{H_s^2}\right), \tag{5.77}$$

where the significant wave height, $H_s \approx 4\sigma$, and σ^2, is the variance of the initial Gaussian field (see formula (2.84) from Chap. 2). In fact, the wave field in shallow water (as well as in deep water) is not Gaussian (see Sect. 5.3), but for the sake of simplicity we will use the assumption of a narrow-band Gaussian process resulting in the Rayleigh distribution for wave heights. For a quasi-monochromatic wave $H = 2A$, the amplitude distribution has the same form as Eq. (5.77). As a result, the exceedance probability functions of the positive (crest) and negative (trough) amplitudes of water oscillations at the vertical wall can be determined explicitly

$$P(R_+) = \exp\left\{-\frac{2}{A_s^2}\left[\frac{R_+}{4} + \frac{1}{2}\left(\sqrt{D+R_+} - D\right)\right]^2\right\}, \tag{5.78}$$

$$P(R_-) = \exp\left\{-\frac{2}{A_s^2}\left[\frac{R_-}{4} - \frac{1}{2}\left(\sqrt{D-R_-} - D\right)\right]^2\right\}, \tag{5.79}$$

where both amplitudes (heights of the crests and troughs) have positive values. For the convenience of graphic representation of the distribution functions, the amplitudes of the water oscillations at the wall will hereafter be normalized by $H_s = 2A_s$, taking into account that the wave amplitude on the wall is within the framework of the linear theory twice the amplitude of the incident wave. In this case, any deviation from the Rayleigh distribution characterizes nonlinear effects, and the main parameter here is $\varepsilon = H_s/D$, which is the natural nonlinear parameter of the shallow-water theory.

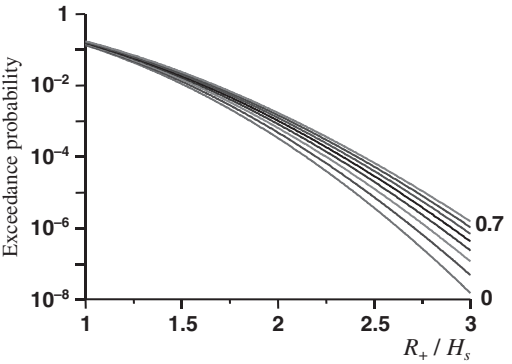

Fig. 5.22 Exceedance probability function of crest heights of water oscillations at the wall. Numbers on curves denote values of $\varepsilon = H_s/D$ with increment of $\varepsilon = 0.1$

Figure 5.22 displays the exceedance probability function of the crest heights of the water oscillations at the wall for different values of the parameter ε, from 0 (linear case) to 0.7 (large-amplitude waves). As it is expected, weak and moderate water oscillations have almost the same Rayleigh distribution as the incident wave, but their crest heights are twice the incident wave amplitudes (this factor is included in the normalization). For extreme waves, including freak waves (their amplitude exceeds twice and more the significant wave height), the probability of the large crests is increased with an increase of the ratio of the significant wave height to water depth. This means that anomalous high crests should occur in the coastal zone more often than in the open sea, and this effect is related to the nonlinear mechanism of wave transformation in the coastal zone. Such waves may overflow through breakwaters and flood the coasts, causing the accidents described in the literature.

In this way, statistical characteristics of trough amplitudes and wave heights are calculated in Pelinovsky et al. (2008). The probability of occurrence of the deepest troughs near the wall is less than the Rayleigh prediction, and therefore freak waves should often have the shape of crests rather than of troughs. Concerning wave height, it can be concluded that nonlinearity decreases the probability of the highest waves compared with the Rayleigh distribution. It means that the probability of meeting unusual high waves for ships and boats near rocks and breakwaters is less than in the open sea, but the shallow water waves may be significantly steeper due to shoaling effects.

5.5.2 Wave Run-up on a Plane Beach

A similar approach can be applied for the process of long wave run-up on a plane beach, defined by the bottom profile function $D(X) = -\alpha X$ (Fig. 5.23). In this case, the nonlinear shallow-water equations (5.65) can be solved with the use of Riemann invariants

$$I_{\pm} = u \pm 2\sqrt{g(D+\eta)} + \alpha T \tag{5.80}$$

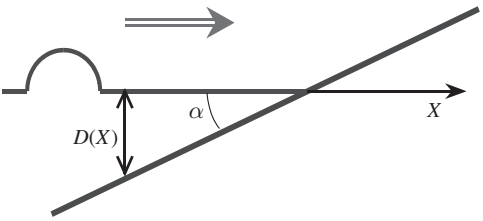

Fig. 5.23 Definition sketch for the wave runup problem

and the Legendre (hodograph) transformation (Carrier and Greenspan 1958). As a result, the long wave run-up process is described by the linear wave equation

$$\frac{\partial^2\Phi}{\partial\lambda^2} - \frac{\partial^2\Phi}{\partial\sigma^2} - \frac{1}{\sigma}\frac{\partial\Phi}{\partial\sigma} = 0, \tag{5.81}$$

and all the physical variables can be expressed through the function $\Phi(\lambda,\sigma)$:

$$\eta = \frac{1}{2g}\left(\frac{\partial\Phi}{\partial\lambda} - u^2\right), \quad u = \frac{1}{\sigma}\frac{\partial\Phi}{\partial\sigma}, \tag{5.82}$$

$$T = \frac{1}{\alpha g}\left(\lambda - \frac{1}{\sigma}\frac{\partial\Phi}{\partial\sigma}\right), \quad X = \frac{1}{2\alpha g}\left(\frac{\partial\Phi}{\partial\lambda} - u^2 - \frac{\sigma^2}{2}\right). \tag{5.83}$$

The physical meaning of the variable σ is the total water depth, and $\sigma = 0$ corresponds to the moving shoreline. Various calculations of the wave field and run-up characteristics using the Carrier-Greenspan transformation can be found in Spielfogel (1976), Pedersen and Gjevik (1983), Synolakis (1987), Pelinovsky and Mazova (1992), Tadepalli and Synolakis (1994), Carrier et al. (2003), Tinti and Tonini (2005), Kânoulu and Synolakis (2006), Didenkulova et al. (2006, 2007), and Didenkulova and Pelinovsky (2008).

A surprising result, which follows from the linear equation (5.81), is that the extreme run-up characteristics (run-up and run-down amplitudes, run-up velocities) can be calculated in the framework of the linear shallow-water theory when the incident wave propagates to the beach from the open sea. Particularly, the run-up amplitude of incident sine wave with amplitude A and frequency Ω given on depth D is

$$\frac{R}{A} = \left(\frac{\pi^2\Omega^2 D}{g\alpha^2}\right)^{1/4}. \tag{5.84}$$

Moreover, the water oscillations on shore are not sinusoidal (see Fig. 5.24). In the figure, cases of various initial amplitudes are shown, expressed through the parameter $Br = R\Omega^2/g\alpha^2$ (condition $Br = 1$ corresponds to wave breaking on shore).

Formulae (5.81), (5.82), (5.83) and (5.84) can be applied to describe the run-up of regular as well as irregular long waves. Due to the implicit character of the Carrier-Greenspan transformation, it is a tricky task to calculate wave characteristics and wave statistics. However, the linear approach may be applied for calculations of the extreme run-up characteristics. Extremes of the Fourier series

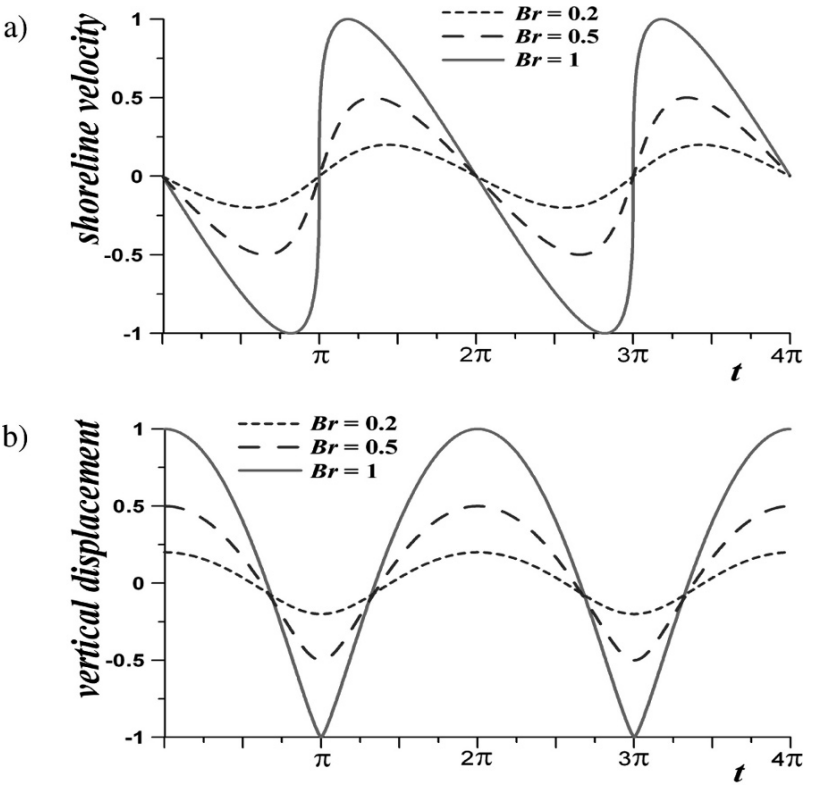

Fig. 5.24 Velocity (**a**) and vertical displacement (**b**) of the moving shoreline

$$\eta(T, X=0) = \left(\frac{16\pi^2\Omega^2 D}{g\alpha^2}\right)^{1/4} \sum_{n=1}^{\infty} \sqrt{n} A_n \sin\left[n\Omega(T-\tau) + \frac{\pi}{4}\right], \tag{5.85}$$

should be obtained for this purpose (Didenkulova et al. 2007, Didenkulova and Pelinovsky 2008). In Eq. (5.85), A_n denotes the spectral amplitudes, Ω is the basic frequency of the incident wave, and τ is the travel time to the coast.

It should be emphasized that series (5.85) can be used when calculating positive and negative run-up amplitudes, but not the moments and distribution functions of the water displacement onshore. Detailed calculations of the distribution functions of the run-up amplitudes are given in(Sergeeva and Didenkulova (2005). For the narrow-band incident wave field, the distribution functions of the run-up characteristics are described by the Rayleigh distribution, as is expected owing to the linearity of the expressions for extreme characteristics. When the spectrum of the incident wave is wider, the distribution functions differ from the Rayleigh law; the mean value of the run-up amplitude changes as well.

The wave field in shallow water involves many coherent wave components. A way to represent such a field as a random set of solitary waves is very popular (see

Brocchini and Gentile 2001). The run-up of a solitary wave on a plane beach is well studied (Synolakis 1987), and the run-up amplitude, R, can be expressed through the soliton amplitude, A, as

$$\frac{R}{D} = 2.8312 \frac{1}{\sqrt{\alpha}} \left(\frac{A}{D} \right)^{5/4}. \tag{5.86}$$

In fact, this formula can be derived from Eq. (5.85) by taking into account the relation between the soliton amplitude and the duration. When the wave field contains random separated solitons, the runup of each individual soliton represents an independent random process and the distribution function of run-up amplitude can be found analytically when the distribution function of the soliton amplitudes is known. Assuming for the sake of simplicity that the Rayleigh distribution for the soliton amplitude, and using (5.86), the exceedance probability of run-up amplitude is

$$P(R) = \exp \left[-0.378 \alpha^{4/5} \frac{(R/D)^{8/5}}{(A/D)^2} \right]. \tag{5.87}$$

The tail of the distribution (5.87) decays slower than that of the Rayleigh distribution. Therefore, the probability of large wave occurrence on coasts is high. More detailed computations of statistical run-up characteristics of the wave field represented by a soliton ensemble are performed in Brocchini and Gentile (2001).

So, the wave run-up on a vertical wall or plane beach leads to an increase of the probability of large-amplitude waves. Thus, a way to reduce possible rogue wave damage should be to include proper coastal protection.

List of Notations

A	wave amplitude
A_s	significant wave amplitude
$b(X,Y)$	distance between neighbouring rays
C	long-wave speed
D	water depth
g	acceleration due to gravity
H	wave height
H_s	significant wave height
$I_{\pm}$	Riemann invariants
k	dimensionless wavenumber
K	wavenumber
l	coordinate along the ray
N_s	soliton number
P	probability distribution function
R	runup amplitude
s	temporal variable
S	non-symmetric wave spectrum

t	dimensionless time
T	time
$\mathbf{u}(X, Y, T)$	depth-averaged velocity
$\mathbf{U} = (U, V)$	fluid velocity in the horizontal plane
Ur	Ursell parameter
V	velocity of the soliton
(x, y)	dimensionless coordinates in the horizontal plane
(X, Y, Z)	coordinates
W	vertical fluid velocity
ε	nonlinear parameter
$\phi(X,Y,Z,T)$	velocity potential
γ	skewness
$\eta(X,Y,T)$	surface elevation
κ	kurtosis
$\widetilde{\kappa}$	normalized kurtosis
λ	wavelength
σ	depth variable in the hodograph transformation
σ	standard deviation, σ^2 is the variance
Ω	cyclic wave frequency
$\zeta(x,y,t)$	dimensionless surface displacement
∇	gradient operator in the horizontal plane

References

Agnon Y, Madsen PA, Schaffer HA (1999) A new approach to high order Boussinesq models. J Fluid Mech 399:319–333

Brocchini M, Gentile R (2001) Modelling the run-up of significant wave groups. Cont Shelf Res 21:1533–1550

Carrier GF, Greenspan HP (1958) Water waves of finite amplitude on a sloping beach. J Fluid Mech 4:97–109

Carrier GF, Wu TT, Yeh H (2003) Tsunami run-up and draw-down on a plane beach. J Fluid Mech 475:79–99

Chen Q, Kirby JT, Dalrymple RA et al (2000) Boussinesq modeling of wave transformation, breaking, and run-up. J Waterway Port Coast Ocean Eng 126:48–56

Didenkulova I, Pelinovsky E (2008) Runup of solitary waves of various shapes on a beach. Oceanology 48:5–10

Didenkulova I, Pelinovsky E, Soomere T, Zahibo N (2007) Runup of nonlinear asymmetric waves on a plane beach. In: Kundu A (ed) Tsunami and Nonlinear Waves, pp 173–188. Springer

Didenkulova II, Zahibo N, Kurkin AA, Levin BV, Pelinovsky EN, Soomere T (2006) Runup of nonlinearly deformed waves on a coast. Dokl Earth Sci 411:1241–1243

Dingemans MW (1996) Water waves propagation over uneven bottom. Vol 2. World Sci, Singapore

Drazin PG, Johnson RS (1989) Solitons: an Introduction. Cambridge University Press, Cambridge

Dysthe KB, Trulsen K, Krogstad HE, Socquet-Juglard H (2003) Evolution of a narrow-band spectrum of random surface gravity waves. J Fluid Mech 478:1–10

Engelbrecht JK, Fridman VE, Pelinovski EN (1988) Nonlinear evolution equations. Longman, London

Fornberg B (1998) A Practical guide to pseudospectral methods. Cambridge University Press, Cambridge

Funakoshi M (1980) Reflection of obliquely incident large-amplitude solitary waves. J Phys Soc Japan 49:2371–2379
Gardner CS, Green JM, Kruskal MD, Miura RM (1967) Method for solving the Korteweg – de Vries equation. Phys Rev Lett 19:1095–1097
Green AE, Naghdi PM (1976) A derivation of equations for wave propagation in water of variable depth. J Fluid Mech 78:237–246
Grimshaw R, Pelinovsky D, Pelinovsky E, Talipova T (2001) Wave group dynamics in weakly nonlinear long-wave models. Phys D 159:35–57
Groesen E, Westhuis JH (2002) Modeling and simulation of surface water waves. Math Comput Simul 59:341–360
Janssen PAEM (2003) Nonlinear four-wave interactions and freak waves. J Phys Oceanogr 33:863–884
Kânoulu U, Synolakis C (2006) Initial value problem solution of nonlinear shallow water-wave equations. Phys Rev Lett 97:148501
Kharif C, Pelinovsky E, Talipova T (2000) Formation de vagues géantes en eau peu profonde. Comptes Rendus de l'Académie des Sciences 328, série Iib:801–807
Kim JW, Bai KJ, Ertekin RC, Webster WC (2003) A strongly-nonlinear model for water waves in water of variable depth – the irrotational Green-Naghdi model. J Offshore Mech Arctic Eng 125:25–32
Kit E, Shemer L, Pelinovsky E, Talipova T, Eitan O, Jiao H (2000) Nonlinear wave group evolution in shallow water. J Waterway Port Cost Ocean Eng 126:221–228
Kokorina A, Pelinovsky E (2005) Numerical simulation of the random waves in shallow water using experimental data. In: Proc 3rd Int Conf APAC (Korea), 1334–1345
Madsen PA, Schaffer HA (1998) Higher-order Boussinesq-type equations for surface gravity waves: derivation and analysis. Phil Trans Roy Soc Lond A 356:3123–3184
Madsen PA, Bingham HB, Liu H (2002) A new Boussinesq method for fully nonlinear waves from shallow to deep water. J Fluid Mech 462:1–30
Madsen PA, Bingham HB, Schaffer HA (2003) Boussinesq-type formulations for fully nonlinear and extremely dispersive water waves: derivation and analysis. Proc Roy Soc Lond A 459:1075–1104
Mase H, Memita T, Yuhi M, Kitano T (2002) Stem waves along the vertical wall due to random wave incidence. Coast Eng 44:339–350
Massel SR (1996a) Ocean surface waves: their physics and prediction. World Scientific Publishing Co Pte Ltd, Singapore
Massel SR (1996b) On the largest wave height in water of constant depth. Ocean Eng 23:553–573
Matveev VB (2002) Positons: slowly decreasing analogues of solitons. Theor Math Phys 131:483–497
Melville WK (1980) On the Mach reflection of solitary waves. J Fluid Mech 98:285–297
Miles JW (1977a) Obliquely interacting solitary waves. J Fluid Mech 79:157–169
Miles JW (1977b) Resonantly interacting solitary waves. J Fluid Mech 79:171–179
Mirchina N, Pelinovsky E (1984) Increase in the amplitude of a long wave near a vertical wall. Izv Atmos Ocean Phys 20:252–253
Murray AC (1978) Solutions of the Korteweg – de Vries equation from irregular data. Duke Math J 45:149–181
Novikov S, Manakov SV, Pitaevskii LP, Zakharov VE (1984) Theory of Solitons: the Inverse Scattering Method. Consult Bureau, New York
Onkuma K, Wadati M (1983) The Kadomtsev – Petviashvili equation, the trace method and the soliton resonance. J Phys Soc Japan 52:749–760
Onorato M, Osborne AR, Serio M, Bertone S (2001) Freak waves in random oceanic sea states. Phys Rev Lett 86:5831–5834
Onorato M, Osborne AR, Serio M, Cavaleri L (2005) Modulational instability and non-Gaussian statistics in experimental random water-wave trains. Phys Fluids 17:078101-1–4
Osborne AR (1995) Solitons in the periodic Korteweg – de Vries equation, the Θ-function representation, and the analysis of nonlinear, stochastic wave trains. Phys Rev E 52:1105–1122

Osborne AR, Serio M, Bergamasco L, Cavaleri L (1998) Solitons, cnoidal waves and nonlinear interactions in shallow-water ocean surface waves. Phys D 123:64–81
Ostrovsky LA, Pelinovsky EN (1975) Refraction of nonlinear ocean waves in a beach zone. Izv Atmos Ocean Phys 11:37–41
Pedersen G, Gjevik B (1983) Runup of solitary waves. J Fluid Mech 142:283–299
Pelinovsky E, Talipova T, Kharif C (2000) Nonlinear dispersive mechanism of the freak wave formation in shallow water. Phys D 147:83–94
Pelinovsky EN (1982) Nonlinear dynamics of tsunami waves. IAP RAS Press, Nizhny Novgorod (In Russian)
Pelinovsky E, Mazova R (1992) Exact analytical solutions of nonlinear problems of tsunami wave run-up on slopes with different profiles. Nat Hazards 6:227–249
Pelinovsky E, Kharif C, Talipova T (2008) Large-amplitude long wave interaction with a vertical wall. Eur J Mech B/Fluids 27:409–418
Pelinovsky E, Sergeeva (Kokorina) A (2006) Numerical modeling of the KdV random wave field. Eur J Mech B/Fluids 25:425–434
Pelinovsky EN (1996) Hydrodynamics of tsunami waves. IAP RAS Press, N Novgorod (In Russian)
Peregrine DH (1967) Long waves on a beach. J Fluid Mech 27:815–827
Peregrine DH (1972) Equaions for water waves and approximations behind them. In: Meyer R (ed) Waves on Beaches. New York Academic Press, New York, pp 95–122
Peterson P, Soomere T, Engelbrecht J, van Groesen E (2003) Interaction solitons as a possible model for extreme waves in shallow water. Nonlin Proc Geophys 10:503–510
Porubov AV, Tsuji H, Lavrenov IV, Oikawa M (2005) Formation of the rogue wave due to nonlinear two-dimensional waves interaction. Wave Motion 42:202–210
Salupere A, Maugin GA, Engelbrecht J, Kalda J (1996) On the KdV soliton formation and discrete spectral analysis. Wave Motion 123:49–66
Salupere A, Peterson P, Engelbrecht J (2002) Long-time behaviour of soliton ensembles. Part 1 – Emergence of ensembles. Chaos Solitons Fractals 14:1413–1424
Salupere A, Peterson P, Engelbrecht J (2003a) Long-time behaviour of soliton ensembles. Part 2 – Periodical patterns of trajectorism. Chaos Solitons Fractals 15:29–40
Salupere A, Peterson P, Engelbrecht J (2003b) Long-time behavior of soliton ensembles. Math Comput Simul 62:137–147
Satsuma J (1976) N-soliton solution of the two-dimensional Korteweg–de Vries equation. J Phys Soc Japan 40:286–290
Sergeeva AV, Didenkulova II (2005) Runup of irregular waves on a plane beach. Proc Ac Eng Sc Russ Fed 14:98–105 (In Russian)
Soomere T, Engelbrecht J (2005) Extreme evaluation and slopes of interacting solitons in shallow water. Wave Motion 41:179–192
Spielfogel LO (1976) Runup of single waves on a sloping beach. J Fluid Mech 74:685–694
Synolakis CE (1987) The runup of solitary waves. J Fluid Mech 185:523–545
Tadepalli S, Synolakis CE (1994) The Runup of N-waves. Proc Roy Soc London A 445:99–112
Talipova T, Kharif C, Giovanangeli J-P (2008) Modelling of rogue wave shapes in shallow water. In: Pelinovsky E, Kharif C (eds) Extreme Ocean Waves, Springer 71–81
Tanaka M (2001) A method of studying of nonlinear random field. Fluid Dyn Res 28:41–60
Tinti S, Tonini R (2005) Analytical evolution of tsunamis induced by near-shore earthquakes on a constant-slope ocean. J Fluid Mech 535:33–64
Toffoli A, Onorato M, Osborne AR, Monbaliu J (2006) Non-gaussian properties of surface elevation in crossing sea states in shallow water. In: Proc Int Coast Eng (ICCE06), 782–790
Wei G, Kirby JT, Grilli ST, Subramanya R (1995) A fully nonlinear Boussinesq model for free surface waves. Part 1: Highly nonlinear unsteady waves. J Fluid Mech 294:71–92
Zabusky NJ, Kruskal MD (1965) Interaction of solutions in a collisionless plasma and recurrence of initial states. Phys Rev Lett 15:240–243
Zakharov VE (1971) Kinetic equation for solitons. Sov J Exp Theor Phys 60:993–1000
Zheleznyak MI, Pelinovsky EN (1985) Physical and mathematical models of the tsunami climbing a beach. In: Tsunami Climbing a Beach. IAP AS Press, Gorky, 8–34